



1 **Hydroclimate variability in Scandinavia over the last millennium - insights from a**
2 **climate model-proxy data comparison**

3 Kristina Seftigen^{1,2,*}, Hugues Goosse², Francois Klein², Deliang Chen¹

4 ¹Regional Climate Group, Department of Earth Sciences, University of Gothenburg, Gothenburg, Sweden.

5 ²Georges Lemaître Centre for Earth and Climate Research (TECLIM), Earth and Life Institute, Université
6 catholique de Louvain (UCL), Belgium.

7 *Corresponding author:

8 E-mail address: kristina.seftigen@gvc.gu.se

9 **Abstract**

10 The integration of climate proxy information with General Circulation Model (GCM) results
11 offers considerable potential for deriving greater understanding of the mechanisms underlying
12 climate variability, as well as unique opportunities for out-of-sample evaluations of model
13 performance. In this study, we combine insights from a new tree-ring hydroclimate
14 reconstruction from Scandinavian with projections from a suite of forced transient simulations
15 of the last millennium and historical intervals from the CMIP5 and PMIP3 archives. Model
16 simulations and proxy reconstruction data are found to broadly agree on the modes of
17 atmospheric variability that produces droughts/pluvials in the region. But despite these
18 dynamical similarities, large differences between simulated and reconstructed hydroclimate
19 time series remain. We find simulated interannual components of variability to be
20 overestimated, while the multidecadal/longer timescale components generally are too weak.
21 Specifically, summertime moisture variability and temperature are weakly negatively
22 associated at inter-annual timescales but positively correlated at decadal timescales, revealed
23 from observational and proxy evidences. On this background, the CMIP5/PMIP3 simulated
24 timescale dependent relationship between regional precipitation and temperature is
25 considerably biased, because the short-term negative association is overestimated, and the
26 long-term relationship is significantly underestimated. The lack of adequate understanding for
27 mechanisms linking temperature and moisture supply on longer timescales has important
28 implication for future projections. Weak multidecadal variability in models also implies that
29 inference about future persistent droughts and pluvials based on the latest generation global
30 climate models will likely underestimate the true risk of these events.



31 **1. Introduction**

32 Among the current key priorities in climate research is a more comprehensive understanding
33 of changes in regional- to continental-scale hydroclimate in response to rising levels of
34 atmospheric greenhouse gases on time scales ranging from decades to centuries (Wu et al.,
35 2013; Hegerl et al., 2015). Delineating the role of internal variability and natural forcing, and
36 its contribution to the anthropogenically forced twentieth century climate (Zhang et al., 2007;
37 Sarojini et al., 2016), is immensely important for attributing past and predicting future
38 trajectories in the hydrological cycle, and for strategic approaches to adaptation and planning.
39 Sparse observational evidences limits possibilities of providing tight constraints on the long-
40 term behavior of the climate system. The longest instrumental records (~150-200 years) are
41 too short to fully sample modes of variability that are either rare or occur on multidecadal-to-
42 centennial timescales. This motivates the development of paleoclimatic proxy reconstructions,
43 which extends the observational baseline into the longer spectrum of climate variability and
44 provides a framework to consider both internal and forced climate changes.

45 Considerable advancements have recently been made in developing tree-ring
46 estimates of late Holocene hydroclimate variability across Scandinavia (Seftigen et al., 2014;
47 Cook et al., 2015). Being located in the high-latitude boreal zone, Scandinavia is well suited
48 for dendroclimatological studies and has a long tradition of climate and environmental
49 research using tree-ring data (Linderholm et al., 2010). The use of tree-ring proxy evidence to
50 study natural hydroclimate variability has however long been secondary when compared to
51 the scientific attention focused on providing local/regional reconstructions (Gunnarson et al.,
52 2011; Esper et al., 2012; McCarroll et al., 2013; Linderholm et al., 2014) and methodologies
53 (Björklund et al., 2012; 2014) to study temperature variability over the last several millennia.
54 Much of the tree-ring research at moisture-limited sites have until recently been limited to a
55 handful of exploratory papers (Helama and Lindholm, 2003; Linderholm et al., 2004; Jönsson
56 and Nilsson, 2009; Drobyshev et al., 2011; Seftigen et al., 2013) that generally develop one or
57 few chronologies to provide local precipitation/drought histories. These studies, together with
58 a steadily growing collection of high-latitude moisture sensitive tree-ring records (e.g.,
59 Seftigen et al., 2015), now serves as a basis for new possibilities to expand the detail and
60 accuracy with which the history of Northern European moisture conditions can be described.
61 A recent milestone in the field include the development of the “Old World Drought Atlas”
62 (“OWDA”, Cook et al., 2015), a set of tree-ring reconstructed year-to-year maps that provide
63 temporal *and* spatial details of droughts and wetness in the last millennium across Europe,



64 including Scandinavia. The OWDA has been used to elucidate hydroclimatic blueprints of the
65 Medieval Climate Anomaly (MCA, ~1000-1200 CE). Aligning with prior findings (Helama et
66 al., 2009), the atlas reveals the occurrence of so-called megadroughts in large portions of
67 continental north-central Europe and southern Scandinavia during the MCA period.
68 Interestingly, MCA and other “Old World” droughts seem to coincide with the timing of
69 some severe and persistent droughts documented in the climate history of North America.
70 While this suggests the presence of some common driving mechanisms across the North
71 Atlantic, being possibly related to variations in the Atlantic Ocean SST or/and the North
72 Atlantic Oscillation (Feng et al., 2011; Oglesby et al., 2012), the cause of these megadroughts
73 remains to be an open question.

74 While the proxy reconstructions undoubtedly play a pivotal role in unraveling
75 statistical qualities of past climate, they are, alone, not able to provide a comprehensive view
76 of the underlying physics governing the climate system. The forced-transient simulations over
77 the last millennium from fully coupled general circulation models (GCMs) (Taylor et al.,
78 2012) therefore offer an important complementary approach to the empirical analyses of
79 proxy estimates. Paleoclimate reconstructions provide an observational basis that spans
80 beyond current climate conditions that were used in developing and tuning such numerical
81 models, thus allowing for out-of-sample evaluations of the models’ predictive power. The
82 models, on the other hand, can be used to explore the dynamics that have driven climate
83 variability in the past.

84 This paper builds on previous tree-ring analyses (Seftigen et al., 2014; 2015) and
85 aims at employing a paleoclimate-data model comparison framework to further explore the
86 drivers and dynamics of drought/pluvials across Northern Europe. We analyze an ensemble of
87 six state-of-the-art GCMs from the Past Model Intercomparison Phase 3 (Schmidt et al., 2011
88 - PMIP3) and the Coupled Model Intercomparison Phase 5 (Taylor et al., 2012 - CMIP5) and
89 compare them to a new regional tree-ring-based proxy reconstruction of drought and wetness,
90 spanning the last millennium of the Common Era (CE). A combined data approach is used to
91 (1) evaluate to what extent the GCMs are capable in reproducing the key features of the
92 paleoclimate record, and (2) to estimate the role of external forcing versus internal variability
93 in driving the hydroclimatic changes regionally. Inter-annual and decadal/longer-term
94 relationships between hydroclimate, and the two key components of rainfall and surface
95 temperature, are also briefly explored and the ability of the CMIP5/PMIP3 models to simulate
96 the mechanisms by which the regional hydroclimate is constrained by these two variables are
97 evaluated. The collective proxy-model data assessment will help to increase our



98 understanding of decadal/longer climate dynamics in regions and to evaluate the ability of the
99 state-of-the-art GCMs to simulate realistic future hydroclimatology regionally and across a
100 variety of different timescales.

101 The paper is structured as follows. Sect. 2 reviews the methods and describes the
102 paleoclimate and CMIP5/PMIP3 datasets. Subsequent analyses concentrates on comparing the
103 GCM simulations with the proxy based hydroclimate reconstructions (sect. 3), and delineating
104 the role of external (sect. 4) and internal (sect. 5) sources of variability over the last
105 millennium. The principal results and the implication of this study are discussed in sect. 6.

106 **2. Data and methods**

107 **2.1 CMIP5/PMIP3 simulations**

108 Simulations with six models (CESM1, CCSM4, IPSL-CM5A-LR, MIROC-ESM, MPI-ESM-
109 P, BCC-CSM1-1) contributing to the Coupled and Paleo Model Intercomparison Projects
110 Phases (CMIP3/PMIP3) (Schmidt et al., 2011; Taylor et al., 2012) have been used (Table I).
111 The analyses were restricted to models that have available complete monthly precipitation and
112 temperature variables spanning the last millennium (850-1849 CE) through historical (1850-
113 2005 CE) time intervals. The six millennium simulations were forced with reconstructed
114 solar, volcanic, greenhouse gas (GHG) and aerosol forcing, and partly land use changes,
115 whereas the historical simulations included natural and anthropogenic forcing (Schmidt et al.,
116 2011; Taylor et al., 2012). Except for CESM1, the analyses were limited to the first r1i1p1
117 ensemble member. Supplementary information (sect. S1, Fig. S1) provide an evaluation of six
118 selected model rainfall and temperature simulations against instrumental reference data
119 focusing on the northern European sector.

120 **2.2. Proxy data**

121 Building on an existing compilation that has previously been used to derive regional
122 spatiotemporal drought climatology (Seftigen et al., 2014; 2015), we analyzed a network of
123 27 *Pinus sylvestris* L. tree-ring width (TRW) chronologies from southern Scandinavia (Fig.
124 1). The start dates of the chronologies varied across the collection, ranging from 532 to 1790
125 CE (Table II). All chronologies extended at least to year 1995. In order to reduce the risk of
126 natural/anthropogenic disturbance signal from inflicting non-climate noise upon the
127 reconstruction, the tree-ring data has been standardized in previous research (Seftigen et al.,
128 2014) by using a flexible “data-adaptive” method of standardization (Cook et al., 1995). This



129 has limited the degree to which longer-timescale climate information can be extracted.
130 Therefore, rather than using the already available hydroclimate reconstruction provided in
131 Seftigen et al. (2014), we have here re-processed the TRW collection with the newest signal-
132 free (SF) method of standardization (Melvin and Briffa, 2008), which has the capacity of
133 preserving long-term variability due to climate changes. The standardization was performed
134 with the ARSTAN software (Cook and Krusic, 2005). Chronologies combining living and
135 historical/subfossil material were standardized with a regional curve standardization (RCS)
136 approach (Briffa et al., 1992), applying a single RCS curve without any pith-offset
137 adjustments to detrend all series. To avoid spurious growth trends in the resulting RCS
138 chronologies stemming from a modern sample bias (Briffa and Melvin, 2011), tree-ring
139 datasets based only on living trees were standardized using the SF method in combination
140 with an age-dependent smoothing spline applied individually to each series. Prior to the
141 standardization, the modern chronology data were high-pass filtered and subsequently
142 grouped by means of a S-mode principal component analysis over the common interval (1792
143 – 1996 CE). The resulting eigenvector loadings are provided in supplemental material (Fig.
144 S2) and describe the major modes of high-frequency variability within the multiple modern
145 chronologies composing the dataset. The subdivision of the chronologies essentially identified
146 an east-west pattern, broadly corresponding to sub-regional differences in topography and
147 climate across the study domain. This suggested that the sub-regional tree-growth coherence
148 at high frequencies was driven by climate. Hence, it would be rational to expect a common,
149 climatically induced, growth variability also at the medium-frequency time scales, while any
150 disparities in the sub-regional tree-growth signal are likely mostly non-climatic in origin (i.e.
151 local site management practices, stand dynamics or other ‘random’ site-specific disturbances).
152 Therefore, in order to remove or minimize undesirable non-climatic noise upon our dataset,
153 modern tree-ring series were first merged group-wise as identified by the first four principal
154 components and subsequently detrended as four separate ‘batches’ using the SF method. The
155 standard version of the resulting tree-growth indices were subsequently separated and
156 averaged for each site to produce individual site chronologies. This procedure enabled us to
157 retain any shared, sub-regional, growth-forcing signal while removing site-specific medium-
158 to high-frequency noise.

159 Final data were adjusted to reduce the variance bias stemming from varying sample
160 size through time (Frank et al., 2006). The resulting chronologies were truncated where the
161 Expressed Population Signal (EPS) (Wigley et al., 1984) dropped below the 0.85 threshold,
162 or, in case of the longer chronologies, at year 1000 CE. The median segment length (MSL) of



163 all the chronologies (Table II) ranged between 74 and 357 years, and the median MSL across
164 all sites was 197 years. Although a precise quantification of returned frequency variance in
165 the final SF detrended tree-ring chronologies was not straightforward, the median MSL
166 suggested that it should be possible to use the network to reconstruct climate variability at
167 time scales up to ~200 years.

168 **2.3. Regional hydroclimatology**

169 The CMIP5/PMIP3 inter-model spread in spatial resolution and sophistication of soil
170 moisture schemes makes meaningful inter-model comparison difficult. To bypass some of
171 these challenges, the Standardized Precipitation Evapotranspiration Index (SPEI) (Vicente-
172 Serrano et al., 2013) was used to characterize the regional hydroclimatology across the study
173 domain. The SPEI, a commonly used metric of soil moisture balance, has successfully been
174 used as a target variable in several prior tree-ring reconstructions (e.g., Seftigen et al., 2014;
175 2015). The index is not a state variable but rather an offline metric of the surface moisture
176 balance that can be consistently derived across models and therefore provide standard
177 measure of hydroclimatic variability across GCMs. The computation of the index is based on
178 normalized monthly climatic water balance, i.e. cumulative precipitation minus potential
179 evapotranspiration (PET), summed over multiple time scales and computed as standard
180 deviations with respect to long-term mean (Vicente-Serrano et al., 2010). The PET was here
181 estimated with the Thornthwaite approach (Thornthwaite, 1948). The method requires surface
182 temperature and latitude data only, and has therefore frequently been used for PET
183 computations over the historical period. Moreover, the choice of methods is motivated by the
184 larger confidence that is placed on GCM simulations of temperature compared to other
185 variables (vapor pressure, wind speed, net radiation, etc.) that are required for more physically
186 based parameterizations of PET. At each grid point, model SPEI were derived from estimated
187 PET and simulated rainfall over the past1000 and historical periods and then standardized
188 against the 1901-2005 normalization period using the SPEI R package version 1.6 (Vicente-
189 Serrano et al., 2010).

190 The proxy dataset was generated by a point-by-point regression (PPR) methodology
191 that was applied to the TRW network to produce a SPEI reconstruction spanning the past
192 millennium. The climate field reconstruction method is based on principal component
193 regression procedure using the TRW chronologies as potential predictors to develop a set of
194 nested multivariate stepwise regression models (see Cook et al., 1999 for details). Here we
195 employed the same calibration/validation scheme, predictor selection and pre-processing steps



196 as previously described in Seftigen et al. (2015). We performed a full period calibration over
197 the 1901-1995 period of TRW/climate data overlap, and a conventional split period
198 calibration/validation procedure (1901-1948 and 1949-1995 periods) for an independent
199 validation of the SPEI estimates. Each nest was centered and scaled to have the same mean
200 and variance as the observational data in the calibration period. The instrumental SPEI target
201 field for the reconstruction was computed from the CRU TS 3.22 (Harris et al., 2014) 0.5°
202 latitude x 0.5° longitude gridded rainfall and temperature datasets over the southern portion of
203 Scandinavia (55° - 65° N and 5° - 30° E) (Fig. 1), using the same conventions as described
204 above. Simple correlation analysis conclusively demonstrated a short-term early summer
205 moisture sensitivity of the TRW records over most of the study domain (Fig. S3). Based on
206 these findings, we selected June SPEI, aggregated over a 2-month time scale, as the target
207 season data for the reconstruction. A final regional time series was averaged from grid points
208 where the calibration regression models explained at least 20% of instrumental variance and
209 the reduction of error (RE) and coefficient of efficiency (CE) (National Research Council,
210 2006) verifications metrics exceeded the generally accepted threshold value of zero across all
211 nests (N = 521 grid points). The mean tree-ring hydroclimate reconstruction (henceforth
212 ScandH17) and the corresponding instrumental target dataset are shown in Fig. 1, and a
213 validation of the reconstruction against 20th century instrumental data that have been withheld
214 from the calibration is provided in supplementary materials (Fig. S4). Results are variable
215 depending on the calibration/validation period used; the validation and calibration statistics
216 are stronger for the 1901-1948 period and substantially weaker for the 1949-1995 period. The
217 most recent and well-replicated nests (mid-1600s to present) are generally explaining the
218 greatest amount of instrumental variance ($R^2 > 40\%$ for the majority of the grid points). A
219 loss of grid cells with declining proxy availability and a drop in reconstruction skill is
220 occurring prior to the late-1400s and subsequently in the 1200s. Point-wise correlation with
221 gridded instrumental SPEI dataset shows that ScandH17 is representative for a larger area in
222 southern and central Scandinavia with a correlation ‘hot spot’ exceeding 0.6 (Fig. 1).

223 **2.4. Analyses**

224 The new proxy-based reconstruction was used to assess the temporal evolution of droughts
225 and pluvials over the last millennium and to elucidate the mechanisms that govern
226 hydroclimate changes in the northern European sector ranging from interannual to
227 multidecadal time scales. We compared regional hydroclimate time-series with the primarily
228 variables governing the moisture balance: precipitation (which supplies moisture) and



229 temperature (which modulates potential evapotranspiration in our method) (sect. 5). The
230 CMIP5/PMIP3 hydroclimate was contrasted against corresponding last-millennium and
231 historical simulations of temperature and precipitation. As there are no independent, annually
232 resolved, proxy reconstructions of rainfall variability currently available for the region, we
233 only included temperature estimates in the comparison with ScandH17. For this purpose, the
234 previously published Linderholm et al. (2014) (hereafter ScandT14) summer temperature
235 reconstruction was used. The two reconstructions ScandH17 and ScandT14 share no common
236 predictors and are thus fully independent, which ensures that any circular statement in the
237 comparison can be ruled out. The ScandT14 record is based on tree-ring maximum density
238 (MXD) and blue intensity data from central-northern Scandinavia and is in terms of signal
239 strength and preserved multi-centennial scale variability one of the best temperature
240 reconstructions currently available for the region.

241 Furthermore, we extended our analyses to the model domain using the methodology
242 of paleoclimate data-model comparison. There were three main components to the combined
243 approach. Firstly, we evaluated the consistency in various datasets and assessed whether the
244 CMIP5/PMIP3 simulations have similar statistical properties as the reconstruction (sect. 3).
245 Spectral and spectral coherency analyses were performed in two ways. The first is the multi-
246 taper approach (Thomson, 1982) based on 4 tapers, where a Monte-Carlo procedure is used to
247 estimate phase 95% confidence limits. We also used the wavelet cohere analyses available in
248 the Grinsted et al. (2004) MATLAB package to assess the frequency dependent relationships
249 and phasing between various datasets.

250 Secondly, we used the Superposed Epoch Analysis (SEA) (Haurwitz and Brier,
251 1981) to evaluate the influence of volcanic aerosol forcing on hydroclimate, temperature and
252 precipitation of the Scandinavian region at inter-annual time scales (sect. 4). For the last
253 millennium, monthly mean volcanic forcing series were obtained from three different sources:
254 Gao et al. (2008), Crowley and Unterman (2013) and Sigl et al. (2015) datasets. We note that
255 the former two forcings have been used as the boundary conditions for the last millennium
256 CMIP5/PMIP3 simulations. The length of the proxy and model data allowed us to include sets
257 of the 20 largest eruptions since 1100 CE (Table III) from the annual forcing series to assess
258 the mean response. For each series and eruption, anomalies for ten post-eruption years were
259 computed relative to a five-year pre-eruption mean. The confidence intervals around the
260 composite responses were determined using a Monte Carlo block resampling ($N = 10\,000$) of
261 the actual event year windows (see Adams et al., 2003 for details).

262 Thirdly, we evaluated the skill of the models to represent the dynamics that drive the



263 variability in hydroclimate of the Scandinavian region by establishing a link between
264 simulated and reconstructed SPEI series and fields of mean sea level pressure (MSLP) over
265 the Atlantic-European sector (sect. 5). Grid point correlations were computed to assess the
266 spatial features and the strength of the teleconnections patterns over the modern era (1950-
267 2005 CE). The analysis was also extended over the last millennium (1000-1849 CE) to
268 investigate the nature of teleconnection stability without the influence of anthropogenic
269 forcing. The gridded monthly instrumental HadSLP2 dataset spanning 1850-present (Allan
270 and Ansell, 2006) was used for comparison with observed and proxy-based estimates of
271 hydroclimate.

272 **3. Modeled and reconstructed hydroclimate series**

273 The regional warm season hydroclimate variability averaged across the six CMIP5/PMIP3
274 models together with the new ScandH17 proxy reconstruction over the last millennium are
275 shown in Fig. 2a-b. Individual model SPEI time series are displayed in Fig. 2c-h. All data
276 have been normalized and centred over the common interval from 1000 to 1995 CE, since this
277 first joint proxy-model comparison focuses on the common relative changes rather than on the
278 magnitude and the absolute values. A simple visual comparison reveals that the models and
279 the reconstruction have generally little agreement in the variance structure and trends. The
280 reconstruction is dominated by a large decadal-to-multidecadal variability while the
281 multimodel mean is relatively flat at these time scales. There are some common features in
282 some of the GCMs and the proxy datasets though (Fig. 2c-h), e.g., the drying in the 19th
283 century, but these are rare when the full millennium is considered and are likely occurring by
284 chance. The historical interval in the proxy record is characterized by a drought in the mid-
285 1800s and a gradual increase in wetness over the 20th century, while, with the exception of
286 short dry episode in the early-1900s, there is no long-term trend in the multimodel mean over
287 the modern era.

288 The very low correlation at inter-annual time scales is to be expected, as the internal
289 variations in the various records represent different realizations of the climate system, which
290 is to a very large extent chaotic at that time scale. The response of each ensemble member to a
291 strong external forcing applied to the model would nevertheless ideally agree (i.e. external
292 punctual perturbations such as volcanic eruptions could induce a coherent short-term
293 response, see sect. 4). Averaging across models or over multiple ensemble members will
294 reduce the contribution from stochastic variability so that the remaining signal can come
295 closer to the model response to external forcing. The comparison between ScandH17 and the



296 multimodel assemble mean reveal, however, no statistically significant agreement between
297 the series, neither on the interannual nor on decadal timescales, suggesting that the simulated
298 hydroclimate changes are not strongly tied to exogenous forcing. Moreover, we found no
299 statistically significant correlation between the different ensemble members in the same
300 model (CESM1) (Fig. 2c), which is the only model providing multiple ensemble members
301 (the only difference among these being the air temperature at the start of each ensemble
302 member (Otto-Bliesner et al., 2016) over the historical and past millennium intervals). The
303 poor overlap between CESM1 ensemble members as well as the individual GCM simulations
304 over the past millennium (despite the use of largely similar forcing series to drive the
305 simulations) is indicative of a larger contribution from internal variability on simulated
306 drought/pluvial occurrence than from changes in exogenous forcing.

307 We compare the spectral properties of the six individual CMIP5/PMIP3 models to
308 the ScandH17 reconstruction, which allows for a general evaluation of potential frequency
309 biases. Fig. 3a confirm that the underlying spectrum of reconstructed hydroclimate variability
310 is significantly redder on decadal-centennial timescales than indicated by the simulated SPEI.
311 In contrast, more hydroclimate variance is concentrated on interannual timescales in the
312 CMIP5/PMIP3 archive than in ScandH17 reconstruction. At frequency bands < 8 years, the
313 power spectral range of most models is systematically above the confidence interval of
314 ScandH17. As a complementary analysis, the numbers of reconstructed and simulated multi-
315 year hydroclimate anomalies greater than a threshold length are compared (Fig. 3d). It is clear
316 that the characteristics of the paleoclimate data are generally not present in the GCM
317 simulations considered here, which suggests that the models are underestimating the risk of
318 persistent multi-year droughts and pluvials in the region. We also consider the agreement
319 between simulated and reconstructed (ScandT14) temperature data in terms of their spectral
320 properties (Fig. 3b). Although the degree of agreement is higher than for hydroclimatology
321 and most models lie within the reconstruction confidence bands, there are some models that
322 have more variance than the reconstruction at periods < 10 years.

323 **4. External sources of variability**

324 Large explosive volcanic eruptions are an important natural radiative forcing mechanism at
325 timescales ranging from seasons to decades (Shindell et al., 2004; Gleckler et al., 2006). The
326 imposed perturbation on the climate system by such events will depend on the nature of the
327 eruption, the magnitude of change in the energy entering the earth's atmosphere, the
328 background climate and internal variability, latitude and season. Analysis of observational



329 data (Shindell et al., 2004), tree-ring records (D'Arrigo et al., 2013) and model simulations
330 (Anchukaitis et al., 2010) indicate a considerable spatial variability in the dynamical response
331 of the climate system to volcanic forcing, with some regions experience surface and
332 tropospheric cooling effects and other regions showing no significant change or even
333 warming effect. Here, we assess the magnitude and timing of Scandinavian summer
334 temperature, rainfall and hydroclimate response to short-term radiative cooling due to
335 volcanic aerosols.

336 A peak cooling is observed one year after the eruption, both in ScandT14 and in the
337 CMIP5/PMIP3 composite average, for all the three forcings considered (Fig. 4). In addition,
338 there is a significant cooling in the year of the event for the Crowley and Unterman (2013)
339 and Sigl et al. (2015) lists. ScandT14 reveal a marginally greater cooling (2.0 °C, mean of the
340 three event lists) than the model average (1.8 °C) one year after the eruption. Remarkably,
341 there is a high degree of similarity in the proxy and in the GCMs not only in terms of the
342 signal timing and the magnitude of the cooling response, but also the rate of recovery. A
343 complete recovery after the volcanic cooling is found two years after the eruption,
344 independent of the forcing list. These results are generally consistent with prior studies
345 (Fischer et al., 2007; Jones et al., 2013; McCarroll et al., 2013) highlighting the importance of
346 explosive volcanism as an external driver of Northern European temperature variability. They
347 also provide a relevant test of the model to radiation perturbations. The agreement between
348 the model simulations and proxy data demonstrates the credibility of the models.

349 Existing research on the response of high-latitude rainfall and hydroclimate to
350 volcanism is limited (in part because high resolution moisture sensitive proxy records are
351 sparse or unavailable). Fischer et al. (2007) found a weak tendency to drying conditions over
352 southern/central Scandinavia in the summer of year 0 and year 1 after the eruption.
353 Circulation changes to the surface cooling were shown to modulate the directly forced
354 response. On continental and global scales, both observational and modeling studies have
355 found a decrease in precipitation (Iles et al., 2013) and streamflow (Iles and Hegerl, 2015) in
356 response to large explosive eruptions, particularly in climatologically humid regions (Carley
357 and Gabriele, 2014). The short-term drying is caused by a reduction in incoming solar
358 radiation reaching the surface, which reduces evaporation, whilst the widespread cooling
359 stabilized the atmosphere and lowers its water holding capacity (Bala et al., 2008). Here, we
360 apply SEA on ScandH17 and simulated SPEI and precipitation to examine the influence of
361 volcanism on Scandinavian moisture availability. A statistically significant reduction in
362 simulated rainfall is observed for all event lists, ranging between the year of the event



363 (Crowley and Unterman, 2013 dataset) and up to two years (Sigl et al., 2015 dataset)
364 following the eruption. We find, however, that the precipitation signal is less consistent across
365 the six CMIP5/PMIP3 models than the cooling effect observed in the simulated temperature
366 series.

367 The SEA on SPEI time series reveals a statistically significant drying after large
368 volcanism. However, the response is more muted than the response of temperature and
369 rainfall separately. Moreover, the agreement between proxy data and the model composite
370 average is weak and there are large inconsistencies between the different forcing records.
371 ScandH17 show a progressive transition from wet conditions in the event year and preceding
372 years to dryer conditions in the consecutive years with significant dry anomalies five
373 (Crowley and Unterman, 2013 dataset) and seven years (Sigl et al., 2015; Gao et al., 2008
374 datasets) after the perturbation. For the CMIP5/PMIP3 multimodel multi-eruption average,
375 only the fifth year after the eruption (Crowley and Unterman, 2013 list) is found to be
376 significantly drier than the adjacent years.

377 The observed weak influence of volcanic forcing on the hydroclimate of the region
378 can be explained by various factors. For example, our results reveal that GCM simulated post-
379 volcanic cooling remains significant for about two years and matches the timescale of the
380 post-volcanic rainfall decrease. Since the SPEI accounts for both supply and demand changes,
381 the net effect would be such that the temperature-driven PET decrease counter a substantial
382 fraction of the precipitation-driven drying, thus producing SPEI values near neutral.
383 Furthermore, the muted response of ScandH17 may arise from autocorrelated biological
384 memory in the TRW data (Esper et al., 2015). The high year-to-year persistence may bias its
385 ability to estimate the abruptness and severity of climatic extremes caused by volcanic
386 cooling. The tree-ring MXD and the blue intensity parameters have, in contrast, been
387 suggested to be superior TRW for recording short term climate perturbations (Wilson et al.,
388 2016), which is likely the reason why the response of ScandT14 is more immediate than that
389 of ScandH17.

390 **5. Internal sources of variability**

391 If the regional hydroclimate variability is indeed dominated by internally generated stochastic
392 components of variability (see sect. 3), atmospheric circulation changes can be the key
393 process shaping regional patterns of moisture availability. Advancing our understanding of
394 the range, stability and strength of teleconnection behavior (defined here as the correlation
395 between hydroclimate and MSLP over the Atlantic-European sector) and its coupling to



396 regional hydroclimate would provide an improved understanding of drought/pluvial dynamics
397 and associated uncertainty. In this section, we first explore major modes of atmosphere
398 variability that impact summertime northern European hydroclimatology. We also assess
399 more extensively the contribution of atmospheric processes (and possible land-atmosphere
400 interactions) by investigating the couplings between hydroclimate and arguably the two most
401 critical variables of the terrestrial climate and the hydrological cycle: precipitation and
402 temperature.

403 To determine the role of teleconnections, correlation of MSLP fields with the
404 hydroclimatic variables over the recent 50 years of the post-industrial era were computed.
405 Results are shown in Fig. 5. As expected, we find that atmospheric dynamics have a
406 significant role in climate variability in the region: a strong correlation with regional
407 hydroclimate is found when MSLP in concurrent months (i.e. May-June) is considered. The
408 results show that the proxy based and CMIP5/PMIP3 simulated dynamics are largely
409 consistent with those in the instrumental record, indicating that both the proxy and the models
410 contain to some degree realistic teleconnections. A consistent feature across the datasets is a
411 tripole structure that would favor increased moisture supply into the Scandinavian region. The
412 structure is characterized by anomalous cyclonic conditions across Scandinavia and high-
413 pressure systems extending over Iceland-Greenland and, albeit less pronounced, over
414 European Russia - Central Asia. Out of the six CMIP5/PMIP3 models, MIROC-ESM is the
415 one showing the largest discrepancy with the major spatial features of the observed
416 correlation map, by failing to reproduce the anti-cyclonic pattern over Iceland-Greenland.
417 Additionally, MIROC-ESM and also CCSM4 show a meridional and zonal shift of the
418 European Russia - Central Asia high-pressure structure towards the Mediterranean region.

419 Atmospheric circulation has been identified as key contributor to recent changes in
420 the climate of Europe in both summer and winter (van Oldenborgh and Van Ulden, 2003;
421 Jones and Lister, 2009). To assess the stationarity of observed MSLP patterns, the analysis
422 was repeated for the pre-industrial last millennium (1000-1849 CE) period (Fig. 6). The
423 exercise was restricted to five GCMs for which simulated MSLP was available for the pre-
424 industrial era (BCC-CSM1-1 was not included). The simulated dynamical relationships were
425 found to be largely stable for all five models, being consistent with observed correlations
426 patterns in the modern era. This suggests a weak influence of anthropogenic forcing on the
427 structure of the dynamical drivers of Scandinavian hydroclimate. In addition to raw data,
428 correlation analysis with 10-year low-passed data was also completed for the pre-industrial
429 period with the purpose to elucidate the drivers of multidecadal hydroclimate variability. We



430 find similar, yet weaker, correlation patterns as compared to the high-frequency variations
431 (results not shown).

432 Precipitation and temperature are the two key variables of the hydrological cycle.
433 Quantifying the covariability between these two variables across various timescales, and the
434 mechanisms that control and modulate it, is therefore of great interest to the study of regional
435 processes on surface energy and water budgets. While past studies have investigated the
436 relationship between temperature and moisture supply in various regions on daily, seasonal
437 and interannual timescales (Adler et al., 2008; Berg et al., 2015; Trenberth, 2011; Madden
438 and Williams, 1978), the nature of concurrent multidecadal/ long-term relationship is still far
439 from being clear. A collective comparison of the new hydroclimate reconstruction with the
440 recently published Linderholm et al. (2014- ScandT14) fully independent warm-season
441 temperature record for Scandinavia is provided in Figs. 7 and 8, in conjunction with the
442 CMIP5/PMIP3 simulations of temperature and rainfall. On interannual timescales, five out of
443 six GCMs show a significant ($p < 0.05$) negative association between simulated interannual
444 temperature and rainfall, with correlation coefficients ranging between $r = -0.12$ and -0.29
445 (1000-2005 CE period). The presence of an anticorrelation on interannual timescales is also
446 found in the instrumental and proxy records, although the anticorrelation is significant in the
447 instrumental record only (Fig. S5).

448 Notably, a frequency dependent relationship between the ScandH17 and ScandT14
449 reconstructions is found. While there is a negative relationship between the two on a year-to-
450 year basis, a simple visual comparison of the two reconstructions shows that they are mostly
451 in phase on decadal and longer timescales (Fig. 7). These results are corroborated by the
452 cross-wavelet coherency analysis (Fig. 8a), revealing that the two reconstructions share
453 significant ($p < 0.05$) in phase variance in multidecadal frequency throughout most of the last
454 millennium. The coupling seems to arise from overlap in shared frequencies at wavelengths
455 longer than ~ 50 years (c.f. Fig. 3). The observed frequency-dependent shift of the
456 relationship thus suggests that cool summers are likely to be rainy summers on a year-to-year
457 basis, while over longer time, warm decades tend to be wet decades in Scandinavia. Notably,
458 our results reveal that the proxy reconstructions and the CMIP5/PMIP3 models portray
459 considerably different relationships between temperature and moisture supply in Scandinavia
460 on longer timescales. We find that the majority of the CMIP5/PMIP3 models are either
461 underestimating or even lacking the positive association between temperature and moisture
462 supply (Fig. 8b - h). The discrepancy appears to arise largely as the result of the spectral
463 inconsistencies among the model and proxy datasets (see sect. 3). While the modeled



464 interannual components of variability are overestimated, the decadal/longer timescale
465 components are generally too weak (Fig. 3).

466 The observed time-dependent shift of the relationship between regional temperature
467 and moisture availability suggests that different mechanisms governing the climate system
468 might be operating at high (interannual) and low (decadal/longer) frequencies, respectively.
469 The previously discussed strong link between inter-annual regional hydroclimate variability
470 and atmospheric pressure patterns suggests that atmospheric dynamics is likely a dominant
471 driver of hydroclimate in the northern European sector on interannual basis. The inverse
472 covariability between warm-season temperature and moisture supply may arise from
473 synoptic-scale correspondence between reduced cloud cover/rainfall and increased incoming
474 shortwave radiation warming the surface during clear sky conditions. In addition, soil
475 moisture exert a strong influence on the allocation of available energy between latent and
476 sensible heating, especially in the warm-season (Seneviratne et al., 2010). Reduced soil
477 moisture, for example, is associated with reduced latent heat flux and thus increased sensible
478 heating and higher air temperatures near the surface. Resulting positive feedbacks of a
479 modified surface heat flux partitioning on cloud cover and radiation (Gentine et al., 2013) and
480 large-scale circulation (Haarsma et al., 2009) could further strengthen the influence of rainfall
481 variability on the thermal climate.

482 The positive association between temperature and moisture supply that is found on
483 decadal-to-multidecadal timescales imply that the long-term regional hydroclimate variability
484 is more sensitive to changes in moisture supply (precipitation) rather than to increased
485 evaporative demand due to warming. It also suggests that the regional moisture balance might
486 be favored by the Clausius-Clapeyron relation (Allen and Ingram, 2002), prescribing an
487 increase in rainfall and intensity of the hydrological cycle during warmer periods in the past
488 millennium. This is generally referred to as ‘wet-get-wetter’/‘dry-get-drier’ mechanism and is
489 attributed to thermodynamics processes (Held and Soden, 2006). In the absence of changes in
490 atmospheric circulation, changes in net moisture supply with warming are related to change in
491 moisture content of the atmosphere. It presupposes that existing circulations will transport
492 more moisture into mesic regions of the globe (e.g., tropics and the mid- to latitudes of
493 Northern Hemisphere), whilst dry regions (e.g., subtropics) will get even dryer, with the
494 fractional change determined by Clausius-Clapeyron relation. In contrast to the proxy records,
495 the model composite average reveals a twentieth-century temperature and rainfall increase yet
496 little change in hydroclimate (Fig. 7b). The multimodel assessment implies that natural
497 variability plays only a subsidiary role in recent changes and that forcing from anthropogenic



498 greenhouse gases (GHG) may have played a more important role (as previously discussed, the
499 effect of GHG-forcing on interannual teleconnection patterns in the modern era seems to be
500 weak). Moreover, the absences of any significant trend in simulated SPEI series indicates that
501 the gains in moisture from increased precipitation are large enough to compensate for any
502 GHG-induced increase in PET in the post-industrial period.

503 **6. Summary and discussion**

504 This study presents the first comprehensive assessment of past variability and trends in
505 hydroclimate of northern European sector over the last millennium of the Common Era along
506 with interrelated variables: precipitation, which supplies moisture, and temperature, which
507 modulates evapotranspiration. A combined approach comparing observational (both
508 instrumental and proxy based) and model-based results is used for evaluation of simulated
509 and real-world interannual-to-centennial climate variability and the underlying physics
510 governing the climate system. A number of important finding emerge from the collective
511 comparison:

512 [1] Models and proxy data are found to broadly agree on the modes of atmospheric variability
513 (sect. 5) that produces droughts and pluvials in Scandinavia. Despite these dynamical
514 similarities, the GCMs are, however, not able to reproduce the hydroclimate features in the
515 proxy record. The droughts and pluvials in the forced simulation are not temporally
516 synchronous with those in the proxy record, nor do the GCM spectra agree with the proxy
517 spectra on the amount of variance present on short and long timescales (sect. 3).

518 [2] The mechanisms that are linking long-term regional summertime moisture variability and
519 temperature are found to be largely missing in the current generation of models (sect. 5). A
520 weak negative association between the two components is revealed from observational and
521 proxy evidences on interannual timescales, while on decadal timescales a positive correlation
522 dominates. The timescale dependent relationship between regional precipitation and
523 temperature is considerably biased in the CMIP5/PMIP3 models, which is reflected in the
524 overestimation of the short-term negative association and significant underestimation of the
525 long-term relationship between them. This discrepancy is most likely arising from the spectral
526 inconsistencies among the model and proxy datasets.

527 [3] There are considerable disagreements among hydroclimate features shown by the
528 CMIP5/PMIP3 simulations (despite the use of largely similar forcing series) (sect. 3).
529 Together, these results point to the possibilities of dominant influence of stochastic processes



530 for the regional hydroclimate and/or deficiencies in the models to realistically represent
531 relevant processes in reality.

532 Essentially, our results reveal that the GCM simulated interannual components of the
533 variability are overestimated, while the multidecadal/longer timescale components are
534 generally too weak. Earlier studies (Ault et al., 2012; Ault et al., 2013) have also argued that
535 most CMIP5/PMIP3 models exhibit less hydroclimate persistence than the instrumental or
536 proxy records. It is difficult to determine explicitly whether it is an external forcing or internal
537 sources that drive the decadal and longer variance in the proxy reconstruction. Prior studies
538 have highlighted the importance of external influences on regional climate variability at
539 different timescales (e.g., Gleckler et al., 2006; Thiéblemont et al., 2015; Sigl et al., 2015).
540 Although we find a short term response of regional hydroclimate to volcanic perturbations
541 (sect. 4), multi-year anomalies in the proxy reconstruction do, however, not appear to
542 correspond well with the epochs following the large volcanic eruptions (e.g., in the 1250s,
543 1450s and 1810s) used to force the models. Thus we cannot rule out that the variability in the
544 reconstruction largely arise from internal sources of variation. Consequently, if the proxy-
545 inferred decadal-to-multidecadal variability is accurate and if the variability is indeed largely
546 unforced, then its magnitude is well beyond what any of the current generation global climate
547 models are able to produce in the region. Underestimation of redness in the models on
548 multidecadal/longer timescales, suggests the GCMs might be lacking/underestimating
549 processes important to the variability at these timescales. There are a number of recognized
550 limitations relating to the dynamics that are relevant to the climatology of the North Atlantic-
551 European sectors. One such example is that models have generally been unable to simulate
552 low-frequency variability in the North Atlantic Oscillation (Osborn, 2004). They have also
553 been shown to underestimate the periodicity of the Atlantic Multidecadal Oscillation
554 (Kavvada et al., 2013), which has implications for the associated hydroclimate impact on
555 neighboring continents (Coats et al., 2015). If, on the other hand, the proxy estimated
556 multidecadal/longer variability in the last millennium is forced by exogenous mechanisms,
557 then either 1) it is a forcing component that is largely missing in the CMIP5/PMIP3 models,
558 alternatively, 2) it is a forcing component that generates a different long-term response in the
559 models compared to the “proxy view” of regional hydroclimatology.

560 It is not possible to pinpoint which part of the disagreement between models and the
561 proxy comes from uncertainties in the tree-ring reconstruction, deficiencies in the forcing
562 series used to drive the models, or from deficiencies in the model. Our analyses have mainly
563 been based on precipitation simulation – a challenging variable for GCMs to simulate



564 accurately. The coarse spatial resolution of the models gives only an approximate
565 representation of the topographic features, which are important for regional hydroclimate.
566 Another possibility is that the scale of the GCMs is unrepresentative of the point estimate
567 provided by the ScandH17 reconstruction. On the other hand, the mismatch between grid box
568 and point estimates is expected to reduce at longer timescales (Jones et al., 1997). There are
569 also limitations of the tree-ring proxy and uncertainties in the interpretation of the data that
570 cannot be ignored. Tree-rings and other biological archives may integrate climate conditions
571 over multiple years (Zhang et al., 2015), which could potentially overestimating the ratio of
572 low to high frequency variability (Franke et al., 2013). While we have been able to establish
573 that prevailing summer moisture availability has been the main growth limitation of trees in
574 the ScandH17 network on an interannual basis over the twentieth century (Figs. S3 and S6),
575 we cannot verify the drought-tree growth model in the pre-instrumental era or across longer
576 spectrum of variability. We are not able to rule out that there might have been climatic
577 regimes in the past that would have caused dynamical shift in the tree growth response to
578 climate, and potentially have called into question the uniformitarian paradigm traditionally
579 applied in the field of dendroclimatology. There are risks that less well know dynamics
580 outside the climate system may introduce variability into the records at decadal/longer
581 timescales. Advances in the mechanistic understanding of the various proxies and the
582 processes through which they record environmental change, e.g., through development and
583 refinement of process-based forward models (Tolwinski-Ward et al., 2011), is currently an
584 emerging priority in the field.

585 The discrepancies in CMIP5/PMIP3 simulated and proxy reconstructed hydroclimate
586 variability in the last millennium is an issue that must be addressed when assessing
587 projections of future hydroclimate change. The lack of adequate understanding for
588 mechanisms linking temperature and moisture supply on longer timescales has important
589 implication for future projections. Weak multidecadal variability in models also implies that
590 inference about future persistent droughts and pluvials based on the latest generation global
591 climate models will likely underestimate the true risk of these events. Reconciliations for the
592 apparent proxy – model mismatch will require efforts from the proxy, modeling and statistics
593 groups, including additional proxy records and refined model simulations of hydroclimate
594 variability in the last millennium, together with the development of alternative approaches for
595 joint proxy-model assessments. Having here provided a first comparison of reconstructed and
596 simulated hydroclimate for Scandinavia, our future efforts will include adaptations of the data
597 assimilation approach to paleoclimate reconstruction. Such efforts hold promise for reducing



598 the uncertainties associated with model physics, external forcings, and internal climate
 599 variability, and ultimately help to refine our view of past and future hydroclimate changes.

600 **Data availability**

601 The raw tree-ring data can be downloaded from the International Tree-Ring Data Bank
 602 (<http://www.ncdc.noaa.gov/paleo/treering.html>) and the SAIMA Tree-Ring Data Bank
 603 (<http://lustiaq.pp.fi/Saima/dendrotieto.htm>) (Table II). The CMIP5/PMIP3 climate model
 604 output can be obtained through the Earth System Grid - Center for Enabling Technologies
 605 (ESG-CET) portal (<http://pcmdi9.llnl.gov/>). The ScandH17 hydroclimate reconstruction is
 606 archived through the NOAA paleoclimate database (citation added on publication).

607 **Acknowledgments**

608 K. Seftigen was supported by the FORMAS mobility starting grant for young researchers
 609 (grant # 2014-723). H. Goosse is senior research associate with the FRS/FNRS, Belgium. The
 610 authors wish to acknowledge the World Climate Research Programme's Working Group on
 611 Coupled Modelling, which is responsible for CMIP, and to thank the climate modeling groups
 612 (listed in Table I of this paper) for producing and making available their model output. For
 613 CMIP the U.S. Department of Energy's Program for Climate Model Diagnosis and
 614 Intercomparison provides coordinating support and led development of software
 615 infrastructure in partnership with the Global Organization for Earth System Science Portals.
 616 The authors also wish to acknowledge the researchers who have produced and made their
 617 tree-ring chronologies available.

618 **References**

- 619 Adams, B. J., Mann, M. E., and Ammann, C. M.: Proxy evidence for an El Niño-like response to
 620 volcanic forcing, *Nature*, 426, 274-278, 2003.
- 621 Adler, R. F., Gu, G., Wang, J.-J., Huffman, G. J., Curtis, S., and Bolvin, D.: Relationships between
 622 global precipitation and surface temperature on interannual and longer timescales (1979–2006),
 623 *Journal of Geophysical Research*, 113, 10.1029/2008jd010536, 2008.
- 624 Allan, R., and Ansell, T.: A New Globally Complete Monthly Historical Gridded Mean Sea Level
 625 Pressure Dataset (HadSLP2): 1850–2004, *Journal of Climate*, 19, 5816-5842, 10.1175/jcli3937.1,
 626 2006.
- 627 Allen, M. R., and Ingram, W. J.: Constraints on future changes in climate and the hydrologic cycle,
 628 *Nature*, 419, 224-232, 2002.
- 629 Anchukaitis, K. J., Buckley, B. M., Cook, E. R., Cook, B. I., D'Arrigo, R. D., and Ammann, C. M.:
 630 Influence of volcanic eruptions on the climate of the Asian monsoon region, *Geophysical Research*
 631 *Letters*, 37, n/a-n/a, 10.1029/2010gl044843, 2010.
- 632 Ault, T. R., Cole, J. E., and St. George, S.: The amplitude of decadal to multidecadal variability in
 633 precipitation simulated by state-of-the-art climate models, *Geophysical Research Letters*, 39, n/a-n/a,
 634 10.1029/2012gl053424, 2012.



- 635 Ault, T. R., Cole, J. E., Overpeck, J. T., Pederson, G. T., St. George, S., Otto-Bliesner, B.,
 636 Woodhouse, C. A., and Deser, C.: The Continuum of Hydroclimate Variability in Western North
 637 America during the Last Millennium, *Journal of Climate*, 26, 5863-5878, 10.1175/jcli-d-11-00732.1,
 638 2013.
- 639 Bala, G., Duffy, P. B., and Taylor, K. E.: Impact of geoengineering schemes on the global
 640 hydrological cycle, *Proceedings of the National Academy of Sciences*, 105, 7664-7669,
 641 10.1073/pnas.0711648105, 2008.
- 642 Berg, A., Lintner, B. R., Findell, K., Seneviratne, S. I., van den Hurk, B., Ducharne, A., Chérut, F.,
 643 Hagemann, S., Lawrence, D. M., Malyshev, S., Meier, A., and Gentine, P.: Interannual Coupling
 644 between Summertime Surface Temperature and Precipitation over Land: Processes and Implications
 645 for Climate Change*, *Journal of Climate*, 28, 1308-1328, 10.1175/jcli-d-14-00324.1, 2015.
- 646 Björklund, J., Gunnarson, B. E., Krusic, P. J., Grudd, H., Josefsson, T., Östlund, L., and Linderholm,
 647 H. W.: Advances towards improved low-frequency tree-ring reconstructions, using an updated *Pinus*
 648 *syvestris* L. MXD network from the Scandinavian Mountains, *Theor Appl Climatol*, 10.1007/s00704-
 649 012-0787-7, 2012.
- 650 Björklund, J., Gunnarson, B. E., Seftigen, K., Esper, J., and Linderholm, H. W.: Blue intensity and
 651 density from northern Fennoscandian tree rings, exploring the potential to improve summer
 652 temperature reconstructions with earlywood information, *Climate of the Past*, 10, 877-885,
 653 10.5194/cp-10-877-2014, 2014.
- 654 Briffa, K. R., Jones, P. D., Bartholin, T. S., Eckstein, D., Schweingruber, F. H., Karlén, W.,
 655 Zetterberg, P., and Eronen, M.: Fennoscandian summers from ad 500: temperature changes on short
 656 and long timescales, *Climate Dynamics*, 7, 111-119, 10.1007/bf00211153, 1992.
- 657 Briffa, K. R., and Melvin, T. M.: A Closer Look at Regional Curve Standardization of Tree-Ring
 658 Records: Justification of the Need, a Warning of Some Pitfalls, and Suggested Improvements in Its
 659 Application, in: *Dendroclimatology: Progress and Prospects*, edited by: Hughes, M. K., Swetnam, T.
 660 W., and Diaz, H. F., Springer Netherlands, Dordrecht, 113-145, 2011.
- 661 Carley, E. I., and Gabriele, C. H.: The global precipitation response to volcanic eruptions in the
 662 CMP5 models, *Environmental Research Letters*, 9, 104012, 2014.
- 663 Coats, S., Cook, B. I., Smerdon, J. E., and Seager, R.: North American Pancontinental Droughts in
 664 Model Simulations of the Last Millennium*, *Journal of Climate*, 28, 2025-2043, 10.1175/jcli-d-14-
 665 00634.1, 2015.
- 666 Cook, E. R., Briffa, K. R., Meko, D., Graybill, D. A., and Funkhouser, G.: The 'segment length curse'
 667 in long tree-ring chronology development for palaeoclimatic studies, *The Holocene*, 5, 229-237, 1995.
- 668 Cook, E. R., Meko, D. M., Stahle, D. W., and Cleaveland, M. K.: Drought Reconstructions for the
 669 Continental United States, *Journal of Climate*, 12, 1145-1162, 1999.
- 670 Cook, E. R., and Krusic, P. J.: Arstan, version 2005, Tree-ring labora- tory, Lamont-Doherty Earth
 671 Obs., Palisades, N. Y. (Available at <http://www.ldeo.columbia.edu/trl>), 2005.
- 672 Cook, E. R., Seager, R., Kushnir, Y., Briffa, K. R., Büntgen, U., Frank, D., Krusic, P. J., Tegel, W.,
 673 van der Schrier, G., Andreu-Hayles, L., Baillie, M., Baittinger, C., Bleicher, N., Bonde, N., Brown, D.,
 674 Carrer, M., Cooper, R., Čufar, K., Dittmar, C., Esper, J., Griggs, C., Gunnarson, B., Günther, B.,
 675 Gutierrez, E., Haneca, K., Helama, S., Herzig, F., Heussner, K.-U., Hofmann, J., Janda, P., Kontic, R.,
 676 Köse, N., Kyncl, T., Levanič, T., Linderholm, H., Manning, S., Melvin, T. M., Miles, D., Neuwirth,
 677 B., Nicolussi, K., Nola, P., Panayotov, M., Popa, I., Rothe, A., Seftigen, K., Seim, A., Svarva, H.,
 678 Svoboda, M., Thun, T., Timonen, M., Touchan, R., Trotsiuk, V., Trouet, V., Walder, F., Ważny, T.,
 679 Wilson, R., and Zang, C.: Old World megadroughts and pluvials during the Common Era, *Science*
 680 *Advances*, 1, 10.1126/sciadv.1500561, 2015.
- 681 Crowley, T. J., and Unterman, M. B.: Technical details concerning development of a 1200 yr proxy
 682 index for global volcanism, *Earth Syst. Sci. Data*, 5, 187-197, 10.5194/essd-5-187-2013, 2013.
- 683 D'Arrigo, R., Wilson, R., and Anchukaitis, K. J.: Volcanic cooling signal in tree ring temperature
 684 records for the past millennium, *Journal of Geophysical Research: Atmospheres*, 118, 9000-9010,
 685 10.1002/jgrd.50692, 2013.
- 686 Drobyshev, I., Niklasson, M., Linderholm, H. W., Seftigen, K., Hickler, T., and Eggertsson, O.:
 687 Reconstruction of a regional drought index in southern Sweden since AD 1750, *The Holocene*, 21,
 688 667-679, 10.1177/0959683610391312, 2011.



- 689 Dufresne, J. L., Foujols, M. A., Denvil, S., Caubel, A., Marti, O., Aumont, O., Balkanski, Y., Bekki,
 690 S., Bellenger, H., Benshila, R., Bony, S., Bopp, L., Braconnot, P., Brockmann, P., Cadule, P., Cheruy,
 691 F., Codron, F., Cozic, A., Cugnet, D., de Noblet, N., Duvel, J. P., Ethé, C., Fairhead, L., Fichefet, T.,
 692 Flavoni, S., Friedlingstein, P., Grandpeix, J. Y., Guez, L., Guilyardi, E., Hauglustaine, D., Hourdin, F.,
 693 Idelkadi, A., Ghattas, J., Joussaume, S., Kageyama, M., Krinner, G., Labetoulle, S., Lahellec, A.,
 694 Lefebvre, M. P., Lefevre, F., Levy, C., Li, Z. X., Lloyd, J., Lott, F., Madec, G., Mancip, M.,
 695 Marchand, M., Masson, S., Meurdesoif, Y., Mignot, J., Musat, I., Parouty, S., Polcher, J., Rio, C.,
 696 Schulz, M., Swingedouw, D., Szopa, S., Talandier, C., Terray, P., Viovy, N., and Vuichard, N.:
 697 Climate change projections using the IPSL-CM5 Earth System Model: from CMIP3 to CMIP5,
 698 *Climate Dynamics*, 40, 2123-2165, 10.1007/s00382-012-1636-1, 2013.
- 699 Esper, J., Frank, D. C., Timonen, M., Zorita, E., Wilson, R. J. S., Luterbacher, J., Holzammer, S.,
 700 Fischer, N., Wagner, S., Nievergelt, D., Verstege, A., and Buntgen, U.: Orbital forcing of tree-ring
 701 data, *Nature Clim. Change*, 2, 862-866, 2012.
- 702 Esper, J., Schneider, L., Smerdon, J. E., Schöne, B. R., and Buntgen, U.: Signals and memory in tree-
 703 ring width and density data, *Dendrochronologia*, 35, 62-70,
 704 <http://dx.doi.org/10.1016/j.dendro.2015.07.001>, 2015.
- 705 Feng, S., Hu, Q., and Oglesby, R. J.: Influence of Atlantic sea surface temperatures on persistent
 706 drought in North America, *Climate Dynamics*, 37, 569-586, 10.1007/s00382-010-0835-x, 2011.
- 707 Fischer, E. M., Luterbacher, J., Zorita, E., Tett, S. F. B., Casty, C., and Wanner, H.: European climate
 708 response to tropical volcanic eruptions over the last half millennium, *Geophysical Research Letters*,
 709 34, n/a-n/a, 10.1029/2006GL027992, 2007.
- 710 Frank, D. C., Esper, J., and Cook, E. R.: On variance adjustments in tree-ring chronology
 711 development, *Tree rings in archaeology, climatology and ecology, TRACE*, 4, 56-66, 2006.
- 712 Franke, J., Frank, D., Raible, C. C., Esper, J., and Bronnimann, S.: Spectral biases in tree-ring climate
 713 proxies, *Nature Clim. Change*, 3, 360-364, 2013.
- 714 Gao, C., Robock, A., and Ammann, C.: Volcanic forcing of climate over the past 1500 years: An
 715 improved ice core-based index for climate models, *Journal of Geophysical Research: Atmospheres*,
 716 113, n/a-n/a, 10.1029/2008JD010239, 2008.
- 717 Gentine, P., Holtlag, A. A. M., D'Andrea, F., and Ek, M.: Surface and Atmospheric Controls on the
 718 Onset of Moist Convection over Land, *Journal of Hydrometeorology*, 14, 1443-1462, 10.1175/jhm-d-
 719 12-0137.1, 2013.
- 720 Gleckler, P. J., Wigley, T. M. L., Santer, B. D., Gregory, J. M., AchutaRao, K., and Taylor, K. E.:
 721 Volcanoes and climate: Krakatoa's signature persists in the ocean, *Nature*, 439, 675-675, 2006.
- 722 Grinsted, A., Moore, J. C., and Jevrejeva, S.: Application of the cross wavelet transform and wavelet
 723 coherence to geophysical time series, *Nonlin. Processes Geophys.*, 11, 561-566, 10.5194/np-11-561-
 724 2004, 2004.
- 725 Gunnarson, B. E., Linderholm, H. W., and Moberg, A.: Improving a tree-ring reconstruction from
 726 west-central Scandinavia: 900 years of warm-season temperatures, *Climate Dynamics*, 36, 97-108,
 727 10.1007/s00382-010-0783-5, 2011.
- 728 Haarsma, R. J., Selten, F., Hurk, B. v., Hazeleger, W., and Wang, X.: Drier Mediterranean soils due to
 729 greenhouse warming bring easterly winds over summertime central Europe, *Geophysical Research*
 730 *Letters*, 36, n/a-n/a, 10.1029/2008GL036617, 2009.
- 731 Harris, I., Jones, P. D., Osborn, T. J., and Lister, D. H.: Updated high-resolution grids of monthly
 732 climatic observations – the CRU TS3.10 Dataset, *International Journal of Climatology*, 34, 623-642,
 733 10.1002/joc.3711, 2014.
- 734 Haurwitz, M. W., and Brier, G. W.: A Critique of the Superposed Epoch Analysis Method: Its
 735 Application to Solar–Weather Relations, *Monthly Weather Review*, 109, 2074-2079, 10.1175/1520-
 736 0493(1981)109<2074:acotse>2.0.co;2, 1981.
- 737 Hegerl, G. C., Black, E., Allan, R. P., Ingram, W. J., Polson, D., Trenberth, K. E., Chadwick, R. S.,
 738 Arkin, P. A., Sarojini, B. B., Becker, A., Dai, A., Durack, P. J., Easterling, D., Fowler, H. J., Kendon,
 739 E. J., Huffman, G. J., Liu, C., Marsh, R., New, M., Osborn, T. J., Skliris, N., Stott, P. A., Vidale, P.-L.,
 740 Wijffels, S. E., Wilcox, L. J., Willett, K. M., and Zhang, X.: Challenges in Quantifying Changes in the
 741 Global Water Cycle, *Bulletin of the American Meteorological Society*, 96, 1097-1115, 10.1175/bams-
 742 d-13-00212.1, 2015.



- 743 Helama, S., and Lindholm, M.: Droughts and rainfall in south eastern Finland since AD 874, inferred
 744 from Scots pine tree-rings, *Boreal Environ Res*, 8, 171-183, 2003.
- 745 Helama, S., Merilainen, J., and Tuomenvirta, H.: Multicentennial megadrought in northern Europe
 746 coincided with a global El Nino-Southern Oscillation drought pattern during the Medieval Climate
 747 Anomaly, *Geology*, 37, 175-178, 10.1130/g25329a.1, 2009.
- 748 Held, I. M., and Soden, B. J.: Robust Responses of the Hydrological Cycle to Global Warming,
 749 *Journal of Climate*, 19, 5686-5699, 10.1175/jcli3990.1, 2006.
- 750 Iles, C. E., Hegerl, G. C., Schurer, A. P., and Zhang, X.: The effect of volcanic eruptions on global
 751 precipitation, *Journal of Geophysical Research: Atmospheres*, 118, 8770-8786, 10.1002/jgrd.50678,
 752 2013.
- 753 Iles, C. E., and Hegerl, G. C.: Systematic change in global patterns of streamflow following volcanic
 754 eruptions, *Nature Geoscience*, 8, 838-842, 10.1038/ngeo2545, 2015.
- 755 Jones, P. D., Osborn, T. J., and Briffa, K. R.: Estimating Sampling Errors in Large-Scale Temperature
 756 Averages, *Journal of Climate*, 10, 2548-2568, 10.1175/1520-0442(1997)010<2548:eseils>2.0.co;2,
 757 1997.
- 758 Jones, P. D., and Lister, D. H.: The influence of the circulation on surface temperature and
 759 precipitation patterns over Europe, *Clim. Past*, 5, 259-267, 10.5194/cp-5-259-2009, 2009.
- 760 Jones, P. D., Melvin, T. M., Harpham, C., Grudd, H., and Helama, S.: Cool North European summers
 761 and possible links to explosive volcanic eruptions, *Journal of Geophysical Research: Atmospheres*,
 762 118, 6259-6265, 10.1002/jgrd.50513, 2013.
- 763 Jönsson, K., and Nilsson, C.: Scots Pine (*pinus sylvestris*L.) on Shingle Fields: A Dendrochronologic
 764 Reconstruction of Early Summer Precipitation in Mideast Sweden, *Journal of Climate*, 22, 4710-4722,
 765 10.1175/2009jcli2401.1, 2009.
- 766 Jungclaus, J. H., Lohmann, K., and Zanchettin, D.: Enhanced 20th-century heat transfer to the Arctic
 767 simulated in the context of climate variations over the last millennium, *Clim. Past*, 10, 2201-2213,
 768 10.5194/cp-10-2201-2014, 2014.
- 769 Kavvada, A., Ruiz-Barradas, A., and Nigam, S.: AMO's structure and climate footprint in
 770 observations and IPCC AR5 climate simulations, *Climate Dynamics*, 41, 1345-1364, 10.1007/s00382-
 771 013-1712-1, 2013.
- 772 Landrum, L., Otto-Bliesner, B. L., Wahl, E. R., Conley, A., Lawrence, P. J., Rosenbloom, N., and
 773 Teng, H.: Last Millennium Climate and Its Variability in CCSM4, *Journal of Climate*, 26, 1085-1111,
 774 10.1175/JCLI-D-11-00326.1, 2012.
- 775 Lehner, F., Joos, F., Raible, C. C., Mignot, J., Born, A., Keller, K. M., and Stocker, T. F.: Climate and
 776 carbon cycle dynamics in a CESM simulation from 850 to 2100 CE, *Earth Syst. Dynam.*, 6, 411-434,
 777 10.5194/esd-6-411-2015, 2015.
- 778 Linderholm, H., and Molin, T.: Early nineteenth century drought in east central Sweden inferred from
 779 dendrochronological and historical archives, *Climate Research*, 29, 63-72, 2005.
- 780 Linderholm, H. W., Niklasson, M., and Molin, T.: Summer Moisture Variability in East Central
 781 Sweden Since the Mid-Eighteenth Century Recorded in Tree Rings, *Geografiska Annaler: Series A*,
 782 *Physical Geography*, 86, 277-287, 10.1111/j.0435-3676.2004.00231.x, 2004.
- 783 Linderholm, H. W., Björklund, J., Seftigen, K., Gunnarson, B. E., Grudd, H., Jeong, J.-H., Drobyshev,
 784 I., and Liu, Y.: Dendroclimatology in Fennoscandia – from past accomplishments to future potential,
 785 *Climate of the Past*, 6, 93-114, 2010.
- 786 Linderholm, H. W., Björklund, J., Seftigen, K., Gunnarson, B. E., and Fuentes, M.: Fennoscandia
 787 revisited: a spatially improved tree-ring reconstruction of summer temperatures for the last 900 years,
 788 *Climate Dynamics*, 45, 933-947, 10.1007/s00382-014-2328-9, 2014.
- 789 Madden, R. A., and Williams, J.: The Correlation between Temperature and Precipitation in the
 790 United States and Europe, *Monthly Weather Review*, 106, 142-147, 10.1175/1520-
 791 0493(1978)106<0142:tcbtap>2.0.co;2, 1978.
- 792 McCarroll, D., Loader, N. J., Jalkanen, R., Gagen, M. H., Grudd, H., Gunnarson, B. E., Kirchhefer, A.
 793 J., Friedrich, M., Linderholm, H. W., Lindholm, M., Boettger, T., Los, S. O., Remmele, S., Kononov,
 794 Y. M., Yamazaki, Y. H., Young, G. H., and Zorita, E.: A 1200-year multiproxy record of tree growth
 795 and summer temperature at the northern pine forest limit of Europe, *The Holocene*, 23, 471-484,
 796 10.1177/0959683612467483, 2013.



- 797 Melvin, T. M., and Briffa, K. R.: A “signal-free” approach to dendroclimatic standardisation,
 798 *Dendrochronologia*, 26, 71-86, [10.1016/j.dendro.2007.12.001](https://doi.org/10.1016/j.dendro.2007.12.001), 2008.
- 799 National Research Council: *Surface Temperature Reconstructions for the Last 2,000 Years*, The
 800 National Academies Press, Washington, DC978-0-309-10225-4, 160, 2006.
- 801 Oglesby, R., Feng, S., Hu, Q., and Rowe, C.: The role of the Atlantic Multidecadal Oscillation on
 802 medieval drought in North America: Synthesizing results from proxy data and climate models, *Global
 803 Planet Change*, 84–85, 56-65, <http://dx.doi.org/10.1016/j.gloplacha.2011.07.005>, 2012.
- 804 Osborn, T. J.: Simulating the winter North Atlantic Oscillation: the roles of internal variability and
 805 greenhouse gas forcing, *Climate Dynamics*, 22, 605-623, [10.1007/s00382-004-0405-1](https://doi.org/10.1007/s00382-004-0405-1), 2004.
- 806 Otto-Bliesner, B. L., Brady, E. C., Fasullo, J., Jahn, A., Landrum, L., Stevenson, S., Rosenbloom, N.,
 807 Mai, A., and Strand, G.: Climate Variability and Change since 850 CE: An Ensemble Approach with
 808 the Community Earth System Model, *Bulletin of the American Meteorological Society*, 97, 735-754,
 809 [10.1175/bams-d-14-00233.1](https://doi.org/10.1175/bams-d-14-00233.1), 2016.
- 810 Sarojini, B. B., Stott, P. A., and Black, E.: Detection and attribution of human influence on regional
 811 precipitation, *Nature Clim. Change*, 6, 669-675, [10.1038/nclimate2976](https://doi.org/10.1038/nclimate2976), 2016.
- 812 Schmidt, G. A., Jungclauss, J. H., Ammann, C. M., Bard, E., Braconnot, P., Crowley, T. J., Delaygue,
 813 G., Joos, F., Krivova, N. A., Muscheler, R., Otto-Bliesner, B. L., Pongratz, J., Shindell, D. T., Solanki,
 814 S. K., Steinhilber, F., and Vieira, L. E. A.: Climate forcing reconstructions for use in PMIP
 815 simulations of the last millennium (v1.0), *Geosci. Model Dev.*, 4, 33-45, [10.5194/gmd-4-33-2011](https://doi.org/10.5194/gmd-4-33-2011),
 816 2011.
- 817 Seftigen, K., Linderholm, H. W., Drobyshev, I., and Niklasson, M.: Reconstructed drought variability
 818 in southeastern Sweden since the 1650s, *International Journal of Climatology*, 33, 2449-2458,
 819 [10.1002/joc.3592](https://doi.org/10.1002/joc.3592), 2013.
- 820 Seftigen, K., Björklund, J., Cook, E. R., and Linderholm, H. W.: A tree-ring field reconstruction of
 821 Fennoscandian summer hydroclimate variability for the last millennium, *Climate Dynamics*, 44, 3141-
 822 3154, [10.1007/s00382-014-2191-8](https://doi.org/10.1007/s00382-014-2191-8), 2014.
- 823 Seftigen, K., Cook, E., Linderholm, H., Fuentes, M., and Björklund, J.: The Potential of Deriving
 824 Tree-Ring-Based Field Reconstructions of Droughts and Pluvials over Fennoscandia, *Journal of
 825 Climate*, 28, 3453-3471, [10.1175/JCLI-D-1300734.s1](https://doi.org/10.1175/JCLI-D-1300734.s1), 2015.
- 826 Seneviratne, S. I., Corti, T., Davin, E. L., Hirschi, M., Jaeger, E. B., Lehner, I., Orlowsky, B., and
 827 Teuling, A. J.: Investigating soil moisture–climate interactions in a changing climate: A review, *Earth-
 828 Science Reviews*, 99, 125-161, <http://dx.doi.org/10.1016/j.earscirev.2010.02.004>, 2010.
- 829 Shindell, D. T., Schmidt, G. A., Mann, M. E., and Faluvegi, G.: Dynamic winter climate response to
 830 large tropical volcanic eruptions since 1600, *Journal of Geophysical Research: Atmospheres*, 109, n/a-
 831 n/a, [10.1029/2003JD004151](https://doi.org/10.1029/2003JD004151), 2004.
- 832 Sigl, M., Winstrup, M., McConnell, J. R., Welten, K. C., Plunkett, G., Ludlow, F., Buntgen, U.,
 833 Caffee, M., Chellman, N., Dahl-Jensen, D., Fischer, H., Kipfstuhl, S., Kostick, C., Maselli, O. J.,
 834 Mekhaldi, F., Mulvaney, R., Muscheler, R., Pasteris, D. R., Pilcher, J. R., Salzer, M., Schupbach, S.,
 835 Steffensen, J. P., Vinther, B. M., and Woodruff, T. E.: Timing and climate forcing of volcanic
 836 eruptions for the past 2,500 years, *Nature*, 523, 543-549, 2015.
- 837 Taylor, K. E., Stouffer, R. J., and Meehl, G. A.: An Overview of CMIP5 and the Experiment Design,
 838 *Bulletin of the American Meteorological Society*, 93, 485-498, [10.1175/bams-d-11-00094.1](https://doi.org/10.1175/bams-d-11-00094.1), 2012.
- 839 Thiéblemont, R., Matthes, K., Omrani, N.-E., Kodera, K., and Hansen, F.: Solar forcing synchronizes
 840 decadal North Atlantic climate variability, *Nature communications*, 6, 8268, 2015.
- 841 Thomson, D. J.: Spectrum estimation and harmonic analysis, *Proceedings of the IEEE*, 70, 1055-1096,
 842 [10.1109/PROC.1982.12433](https://doi.org/10.1109/PROC.1982.12433), 1982.
- 843 Thornthwaite, C. W.: An Approach Toward a Rational Classification of Climate, *Soil Science*, 66, 77,
 844 1948.
- 845 Tolwinski-Ward, S., Evans, M. N., Hughes, M. K., and Anchukaitis, K. J.: An efficient forward model
 846 of the climate controls on interannual variation in tree-ring width, *Climate Dynamics*, 36, 2419-2439,
 847 [10.1007/s00382-010-0945-5](https://doi.org/10.1007/s00382-010-0945-5), 2011.
- 848 Trenberth, K. E.: Changes in precipitation with climate change, *Climate Research*, 47, 123-138,
 849 [10.3354/cr00953](https://doi.org/10.3354/cr00953), 2011.



- 850 van Oldenborgh, G. J., and Van Ulden, A. A. D.: On the relationship between global warming, local
851 warming in the Netherlands and changes in circulation in the 20th century, *International Journal of*
852 *Climatology*, 23, 1711-1724, 10.1002/joc.966, 2003.
- 853 Vicente-Serrano, S. M., Beguería, S., and López-Moreno, J. I.: A Multiscalar Drought Index Sensitive
854 to Global Warming: The Standardized Precipitation Evapotranspiration Index, *Journal of Climate*, 23,
855 1696-1718, 10.1175/2009jcli2909.1, 2010.
- 856 Vicente-Serrano, S. M., Gouveia, C., Camarero, J. J., Beguería, S., Trigo, R., López-Moreno, J. I.,
857 Azorín-Molina, C., Pasho, E., Lorenzo-Lacruz, J., Revuelto, J., Morán-Tejeda, E., and Sanchez-
858 Lorenzo, A.: Response of vegetation to drought time-scales across global land biomes, *Proceedings of*
859 *the National Academy of Sciences*, 110, 52-57, 10.1073/pnas.1207068110, 2013.
- 860 Watanabe, S., Hajima, T., Sudo, K., Nagashima, T., Takemura, T., Okajima, H., Nozawa, T., Kawase,
861 H., Abe, M., Yokohata, T., Ise, T., Sato, H., Kato, E., Takata, K., Emori, S., and Kawamiya, M.:
862 MIROC-ESM 2010: model description and basic results of CMIP5-20c3m experiments, *Geosci.*
863 *Model Dev.*, 4, 845-872, 10.5194/gmd-4-845-2011, 2011.
- 864 Wigley, T. M. L., Briffa, K. R., and Jones, P. D.: On the Average Value of Correlated Time Series,
865 with Applications in Dendroclimatology and Hydrometeorology, *Journal of Climate and Applied*
866 *Meteorology*, 23, 201-213, 10.1175/1520-0450(1984)023<0201:otavoc>2.0.co;2, 1984.
- 867 Wilson, R., Anchukaitis, K., Briffa, K. R., Büntgen, U., Cook, E., D'Arrigo, R., Davi, N., Esper, J.,
868 Frank, D., Gunnarson, B., Hegerl, G., Helama, S., Klesse, S., Krusic, P. J., Linderholm, H. W.,
869 Myglan, V., Osborn, T. J., Rydval, M., Schneider, L., Schurer, A., Wiles, G., Zhang, P., and Zorita, E.:
870 Last millennium northern hemisphere summer temperatures from tree rings: Part I: The long term
871 context, *Quaternary Science Reviews*, 134, 1-18, 10.1016/j.quascirev.2015.12.005, 2016.
- 872 Wu, P., Christidis, N., and Stott, P.: Anthropogenic impact on Earth's hydrological cycle, *Nature*
873 *Clim. Change*, 3, 807-810, 2013.
- 874 Wu, T., Song, L., Li, W., Wang, Z., Zhang, H., Xin, X., Zhang, Y., Zhang, L., Li, J., Wu, F., Liu, Y.,
875 Zhang, F., Shi, X., Chu, M., Zhang, J., Fang, Y., Wang, F., Lu, Y., Liu, X., Wei, M., Liu, Q., Zhou,
876 W., Dong, M., Zhao, Q., Ji, J., Li, L., and Zhou, M.: An overview of BCC climate system model
877 development and application for climate change studies, *Journal of Meteorological Research*, 28, 34-
878 56, 10.1007/s13351-014-3041-7, 2014.
- 879 Zhang, H., Yuan, N., Esper, J., Werner, J. P., Xoplaki, E., Büntgen, U., Treydte, K., and Luterbacher,
880 J.: Modified climate with long term memory in tree ring proxies, *Environmental Research Letters*, 10,
881 084020, 10.1088/1748-9326/10/8/084020, 2015.
- 882 Zhang, X., Zwiers, F. W., Hegerl, G. C., Lambert, F. H., Gillett, N. P., Solomon, S., Stott, P. A., and
883 Nozawa, T.: Detection of human influence on twentieth-century precipitation trends, *Nature*, 448, 461-
884 465, 2007.
- 885
- 886
- 887
- 888
- 889
- 890
- 891
- 892



893 **Tables and figures**

894 **Table I.** CMIP5/PMIP3 model description.

Model Name	Resolution [Atmosphere]	Resolution [Ocean]	Reference
CCSM4	192 x 288	384 x 320	Landrum et al. (2012)
CESM1	96 x 144	384 x 320	Lehner et al. (2015)
IPSL-CM5A-LR	96 x 96	149 x 182	Dufresne et al. (2013)
MIROC-ESM	64 x 128	192 x 256	Watanabe et al. (2011)
MPI-ESM-P	96 x 192	220 x 256	Jungclaus et al. (2014)
BCC-CSM1-1	64 x 128	232 x 360	Wu et al. (2014)

895 **Table II:** Tree-ring network description.

Site	Coord.	Time coverage	Standardization method	MSL ³	Source
Eastern Finland	61.87N, 28.90E	535 -2002 CE	RCS ¹	147 yrs	Helama et al. (2009) Online resource: http://lustiag.pp.fi/Saima/dendrotieto.htm Date access: January 2013
Gotland Sweden	57.49N, 18.41E	1127-2011 CE	RCS	130 yrs	Investigator: Schweingruber, F.H. Online resource: https://www.ncdc.noaa.gov/paleo/study/4427 Date access: January 2013 Updated in Seftigen et al. (2015)
Jondalen Norway	59.71N, 9.53E	1185 -2011 CE	RCS	165 yrs	Investigator: Briffa, K. Online resource: https://www.ncdc.noaa.gov/paleo/study/2826 Date access: January 2013 Updated in Seftigen et al. (2015)
Baljåsen Sweden	59.04N, 12.27E	1686-2002 CE	SF2 ²	174 yrs	Seftigen et al. (2015)
Björbo Sweden	60.27N, 14.44E	1450-2011 CE	SF	177 yrs	Investigator: Axelsson, T. Online resource: https://www.ncdc.noaa.gov/paleo/study/2667 Date access: January 2013
Ekhultebergen Sweden	57.45N, 13.50E	1705-2008 CE	SF1	215 yrs	Seftigen et al. (2015)
Färhagsberget Sweden	58.08N, 16.14E	1621-2011 CE	SF1	262 yrs	Seftigen et al. (2015)
Helvetets håla Sweden	57.14N, 16.14E	1691-2011 CE	SF1	255 yrs	Seftigen et al. (2015)
Halle-Vagnaren Sweden	57.17N, 15.17E	1718-2009 CE	SF3	186 yrs	Seftigen et al. (2015)
Hornslandet Sweden	59.01N, 11.08E	1590-2011 CE	SF1	270 yrs	Seftigen et al. (2015)
Korphälorna Sweden	61.43N, 17.00E	1790-2011 CE	SF1	199 yrs	Seftigen et al. (2015)
Myrkaby Sweden	57.45N, 15.23E	1669-2011 CE	SF2	294 yrs	Seftigen et al. (2015)
Nämndö Sweden	59.52N, 16.56E	1582-1995 CE	SF1	123 yrs	Investigator: Larsson, L. Online resource: https://www.ncdc.noaa.gov/paleo/study/3869 Date access: January 2013
Valekleven-Ombo Sweden	59.11N, 18.41E	1578-2011 CE	SF1	225 yrs	Seftigen et al. (2015)
Putbergen Sweden	58.37N, 14.32E	1734-2008 CE	SF1	188 yrs	Seftigen et al. (2015)
Salboknös Sweden	59.11N, 16.55E	1486-2011 CE	SF2	357 yrs	Seftigen et al. (2015)
Särö Sweden	61.92N, 11.93E	1712-2002 CE	SF3	176 yrs	Seftigen et al. (2015)
Sisshammer Sweden	59.46N, 14.54E	1661-2003 CE	SF	74 yrs	Investigator: Andreason, T. Online resource: https://www.ncdc.noaa.gov/paleo/study/2663 Date access: January 2013
Skärmarbodabergen Sweden	57.51N, 11.93E	1600-2002 CE	SF3	160 yrs	Seftigen et al. (2015)
Skitåsen Sweden	59.09N, 18.02E	1672-2011 CE	SF2	285 yrs	Seftigen et al. (2015)
Skuleskogen Sweden	59.26N, 15.07E	1448-2011 CE	SF	181 yrs	Seftigen et al. (2015)
Sörknatten Sweden	59.22N, 15.29E	1762-2009 CE	SF3	197 yrs	Seftigen et al. (2015)
Tjurhults mosse Sweden	63.06N, 18.29E	1655-2011 CE	SF2	268 yrs	Seftigen et al. (2015)
Tjusthult Sweden	58.55N, 12.27E	1681-2011 CE	SF1	221 yrs	Seftigen et al. (2015)
Tyresta Sweden	59.52N, 14.71E	1609-2010 CE	SF1	198 yrs	Linderholm and Molin (2005) Updated in Seftigen et al. (2015)

896 ¹ RCS: Regional Curve Standardization;897 ² SF: Signal-Free Standardization. The number after the abbreviation indicates the PCA cluster number (Fig. S2);898 ³MSL: Mean Segment Length.



899 **Table III.** Event years used in the Superposed Epoch Analysis (Fig. 4). The event lists are composed
 900 of the 20 strongest eruptions from each record.

Source	Event years (CE)
Gao et al. (2008) (sulfate aerosol > 15 Tg)	1167, 1176, 1195, 1227, 1258, 1284, 1328, 1452, 1459, 1584, 1600, 1641, 1719, 1783, 1809, 1815, 1831, 1835, 1991
Crowley and Unterman (2013) (AOD > 0.13)	1229, 1258, 1259, 1286, 1287, 1456, 1457, 1600, 1601, 1641, 1695, 1696, 1809, 1810, 1815, 1816, 1817, 1884, 1992
Sigl et al. (2015) (global forcing < 5.86 W/m ²)	1108, 1171, 1191, 1230, 1258, 1276, 1286, 1345, 1453, 1458, 1601, 1641, 1695, 1783, 1809, 1815, 1832, 1836, 1992

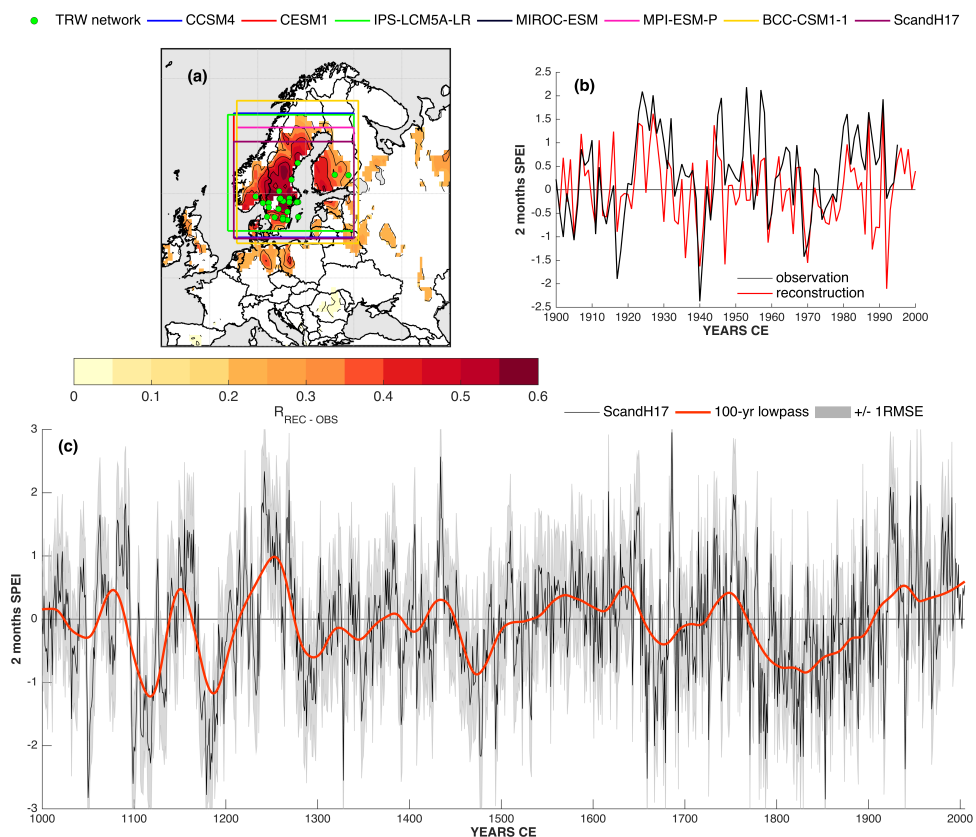


Figure 1: Average regional SPEI time series reconstructed from tree-rings. (a) Location of the tree-ring network used for regional reconstruction and the extent of the CMIP5/PMIP3 model precipitation and temperature grids used to derive regional SPEI estimates. Shaded contours display the correlation ($p < 0.1$) between the tree-ring reconstruction and fields of instrumental SPEI data over the 1901-1995 period; (b) average regional reconstructed and instrumental 20th century 2-month June SPEI; (c) average regional SPEI nested reconstruction, with the ± 1 RMSE of the regression equations outlined in grey shading. A smoothed version of the reconstruction using a 100-year loess smooth is shown in red. Reconstruction assessment metrics are provided in supplementary materials (Fig. S4).

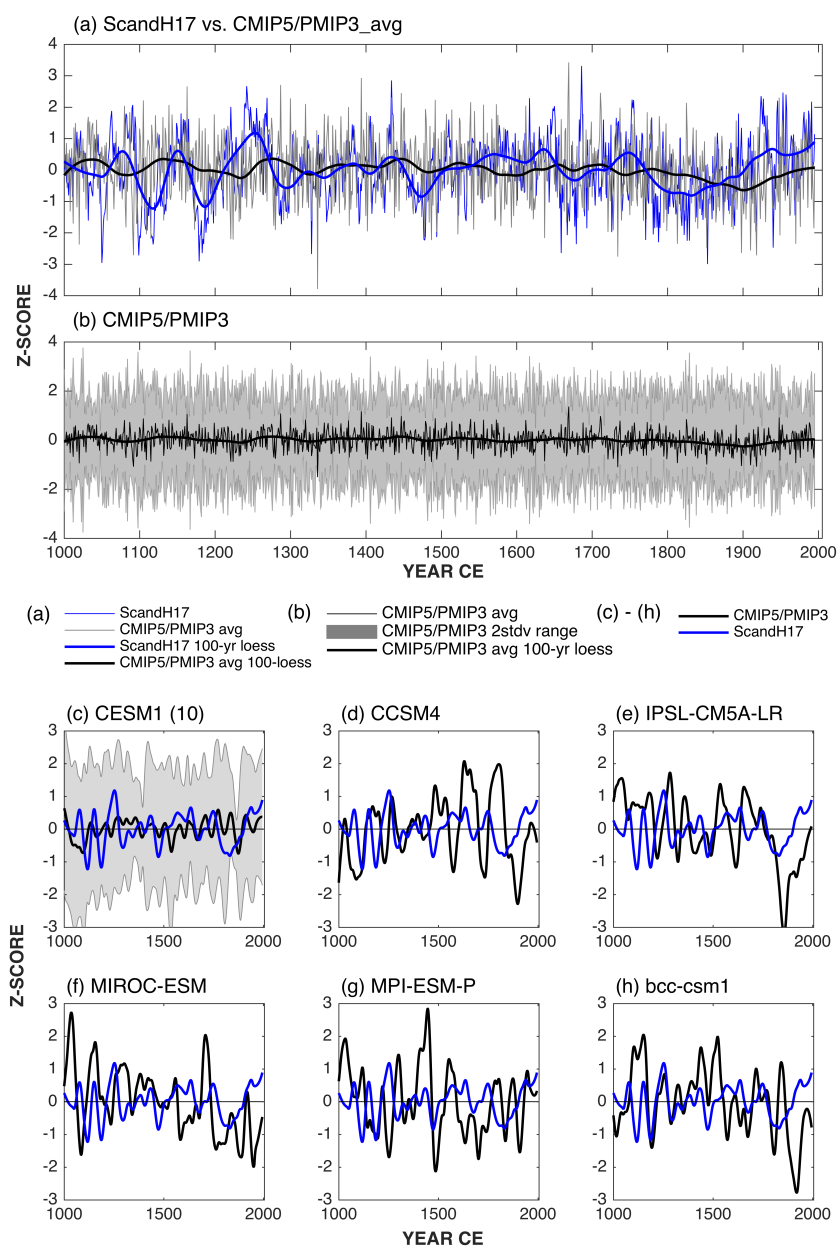


Figure 2: Comparison of reconstructed SPEI with forced model runs. (a) The reconstruction versus the mean of the six CMIP5/PMIP3 models transformed into standard normal deviates (z-scores) over the 1000-1995 CE period and smoothed with 100-year loess filter; (b) multimodel mean and the two standard deviation range (shading) of the six GCMs; (c) mean and two standard deviation (shading) of CESM1 ten smoothed and z-scored ensemble members (blue) together; (d) – (h) the



reconstruction (blue) versus individual model runs (black). All time series have been smoothed with 100-year loess filter and then z-scored over the 1000-1995 CE period.

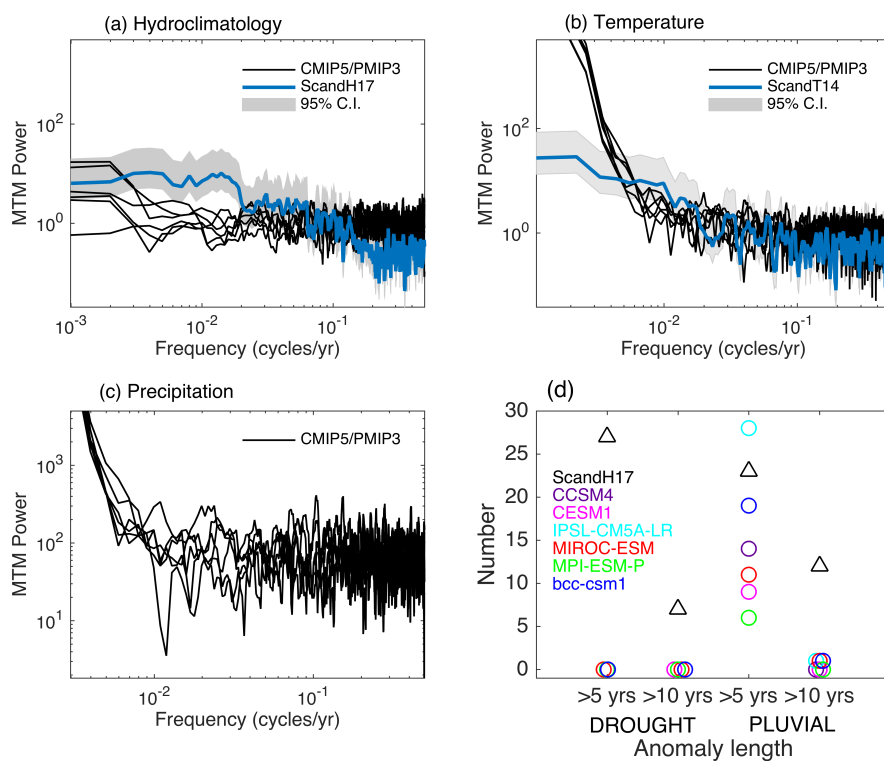


Figure 3: Spectral properties (multi-taper approach, 4 tapers) of (a) SPEI, (b) temperature and (c) precipitation over the common 1100-1995 period. For SPEI and temperature, the spectral properties of individual GCMs (r1i1p1 ensemble) are compared to those of the tree-ring ScandH17 and ScandT14 reconstructions. Shaded areas show the 95% confidence interval of the reconstruction spectra. (d) The number of droughts and pluvials in the reconstructed and simulated time series that are > 5 and >10 years in duration. Spectral properties of the individual models are provided in Fig. S7.

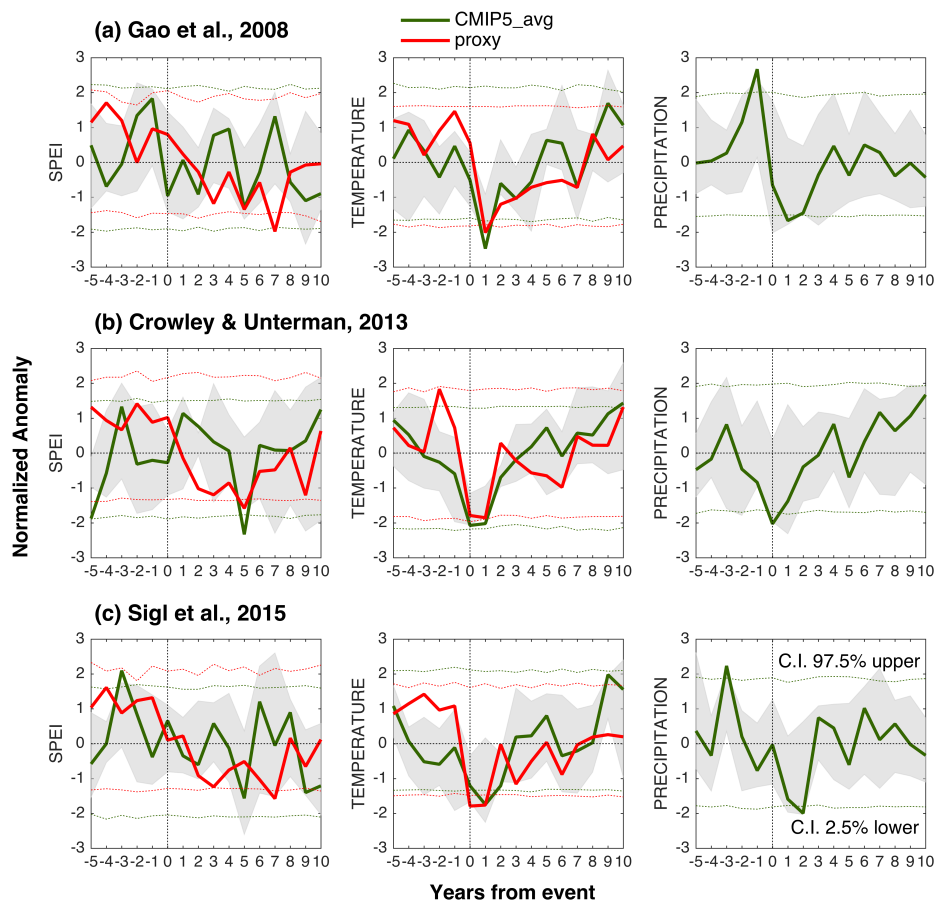


Figure 4: Modeled and reconstructed hydroclimate response to eruptions. Superposed epoch analysis using the 20 largest eruption years from the (a) Gao et al. (2008), (b) Crowley and Unterman (2013), and (c) Sigl et al. (2015). Table III lists the event years used in the analysis. Grey shading indicate the range of modeled hydroclimate response from the six GCMs. Confidence intervals (C.I.) are derived from bootstrap resampling ($N = 10\,000$).

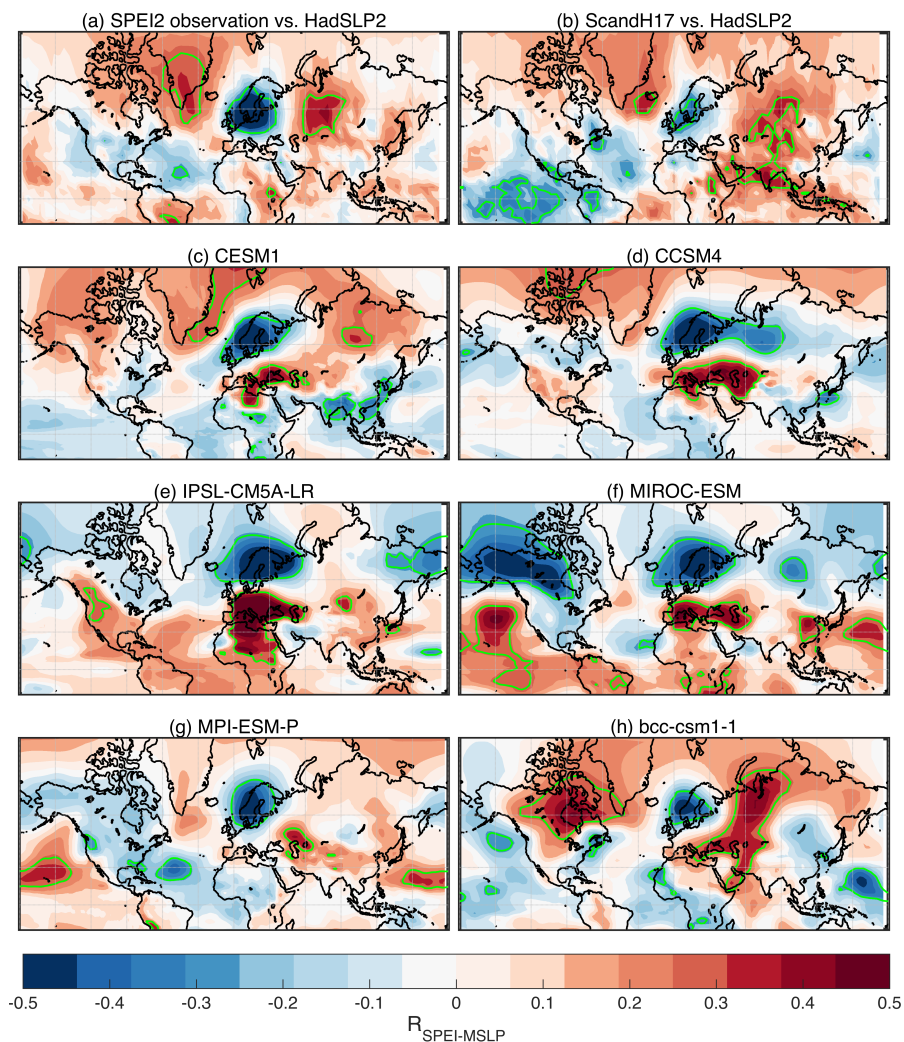


Figure 5: Spatial distribution of correlation coefficient of northern European warm season hydroclimate and mean sea level pressure (MSLP). Association between regional drought index and sea level pressure over the 1950-1995 period. (a) observational, (b) ScandH17, (c)-(g) model based results (including r1i1p1 ensemble only). Regions with significant ($p < 0.05$) correlations are outlined in green contours.

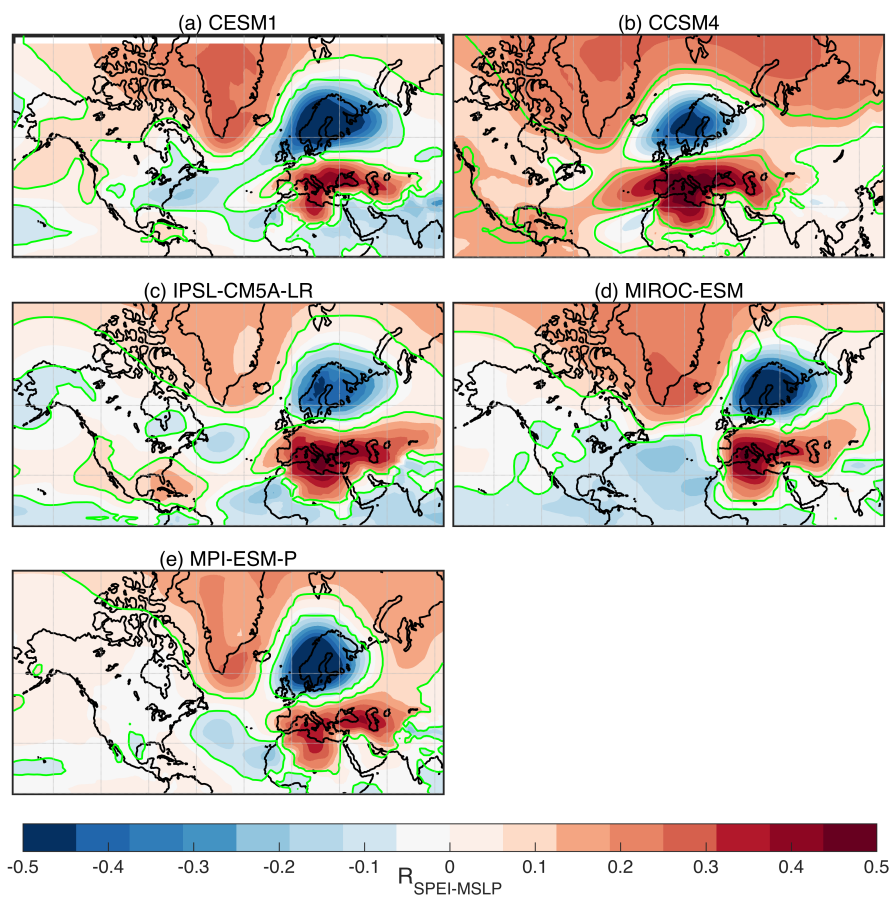


Figure 6: Spatial distribution of correlation coefficient of northern European warm season hydroclimate and mean sea level pressure (MSLP). Same as Fig. 5, but for the 850-1849 CE period.

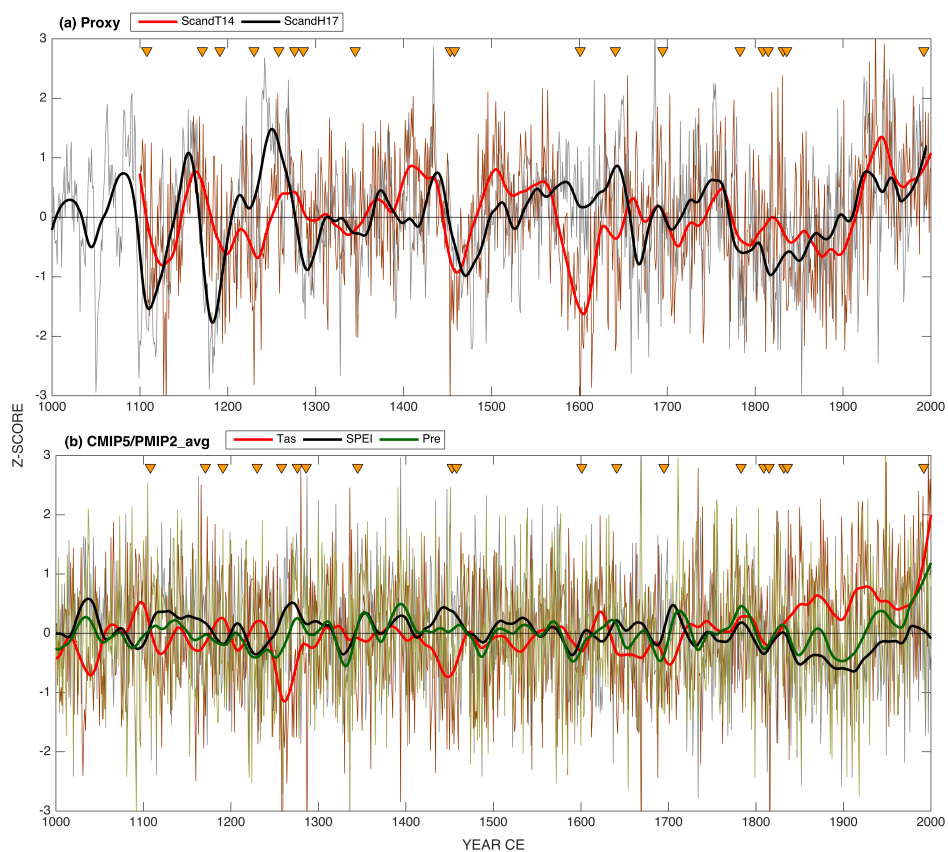


Figure 7: Time series of (a) ScandH17 and ScandT14, and (b) GCM (r1i1p1 ensemble) average temperature, precipitation and SPEI. Smoothed time-series using a 50-year loess filter are shown as thick lines. Individual model data are provided in supplementary material (Fig. S8). The years with volcanic eruptions from Table III are indicated by triangle glyphs.

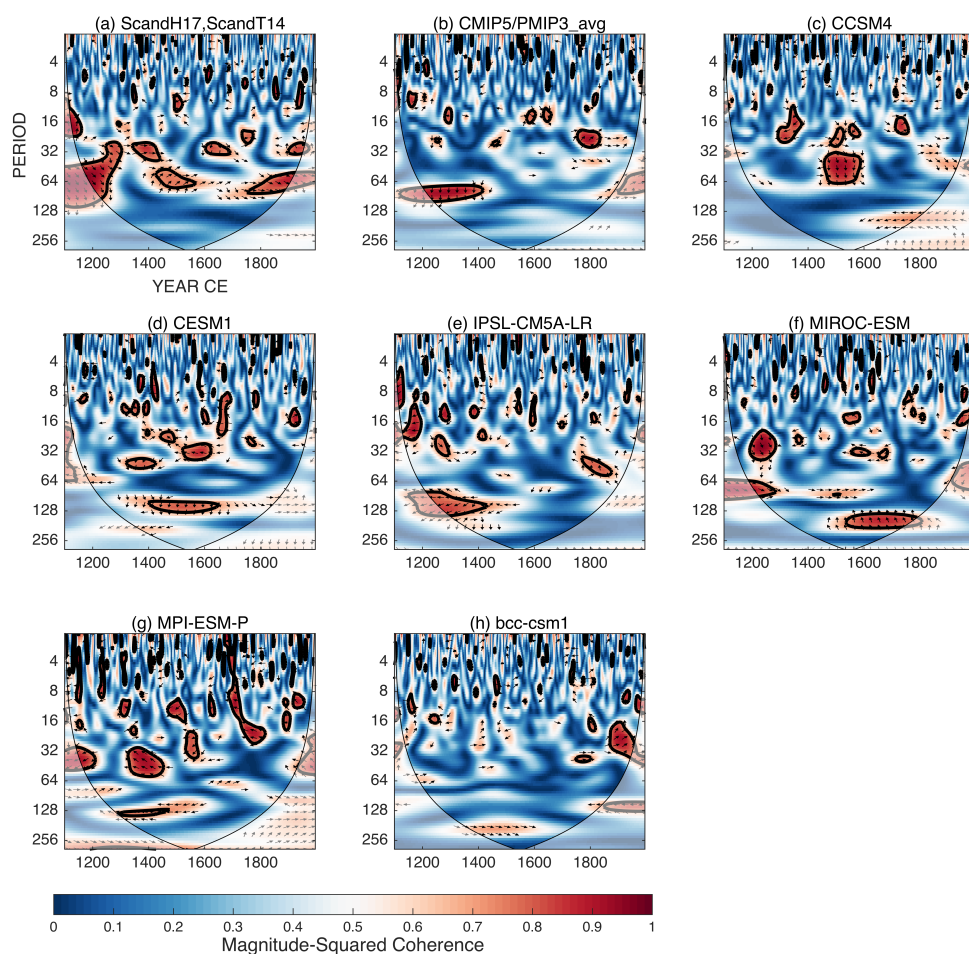


Figure 8: Squared wavelet coherence and phase between (a) ScandH17 and ScandT14, and (b) – (h) CMIP5/PMIP3 simulations of temperature and rainfall. The arrows indicate the relative phase relationship between two series; right (left) pointing arrow indicates in-phase (180 degrees out of phase) relationship. Significant coherence at 95% significance level is shown as thick contour.